

1 A new inventory of High Mountain Asia ~~surge-type~~surging glaciers 2 derived from multiple elevation datasets since the 1970s

3 Lei Guo¹, Jia Li¹, Amaury Dehecq², Zhiwei Li¹, Xin Li³, Jianjun Zhu¹

4 ¹School of Geo-science and Info-physics, Central South University, Changsha, 410083, China.

5 ²Univ. Grenoble Alpes, IRD, CNRS, Grenoble INP, IGE, Grenoble, 38000, France.

6 ³Institute of Tibetan Plateau Research, Chinese Academy of Sciences, Beijing, 100101, China.

7

8 Correspondence to: Jia Li (lijia20050710@csu.edu.cn)

9 **Abstract.** ~~Surges are~~Glacier surging is an ~~important source~~unusual undulation of ~~glacier hazards~~ice flow and complete ~~surge-~~
10 ~~typesurging~~ glacier inventories are ~~required~~important for ~~regional mass balance studies and~~ assessing glacier-related hazards.
11 Glacier surge events in High Mountain Asia (HMA) are widely reported. However, the completeness of present inventories of
12 HMA ~~surge-type~~surging glaciers is constrained by the insufficient spatial and temporal coverage of glacier change
13 observations, or by the limitations of the identification methods. In this paper, we established a new inventory of HMA ~~surge-~~
14 ~~typesurging~~ glaciers based on the glacier surface elevation ~~changes and morphological~~ changes over four decades. Four kinds
15 of elevation sources (KH-9 DEM, NASADEM, COP30 DEM, HMA8m DEM), ~~three elevation change datasets, and long-~~
16 ~~term Landsat image series~~ were utilized to ~~estimate~~access the ~~glacier surface elevation changes~~ distinctive change patterns of
17 ~~surging glaciers~~ during two periods (1970s-2000 and 2000-~~2010s~~2020). In total ~~404~~5890 ~~surging and 336~~ surge-~~typelike~~
18 glaciers were identified in HMA. Compared to the ~~latest surge-type~~previous surging glacier ~~inventory~~inventories in HMA, our
19 inventory incorporated ~~477~~more new ~~surge-type~~surging glaciers. The number and area of ~~surge-type~~surging glaciers accounted
20 for ~2.49% (excluding glaciers less than 0.~~34~~ km²) and ~~~23.32~~16.59% of the total glacier number and glacier area in HMA,
21 respectively. ~~Considering that glacier outlines are usually composed of multiple tributaries within a glacier complex, the~~
22 ~~proportion of surge-related area may be overestimated, and the number of surge-type glaciers could be even larger. Surge-type~~
23 ~~glaciers~~Glacier surges were found in 21 of the 22 subregions of HMA (except for the Dzhungarsky Alatau), however, the
24 density of ~~surge-type glaciers~~surging glacier is highly uneven. ~~Surge-type~~Surging glaciers are common in the northwest
25 subregions (e.g., Pamir and Karakoram), but scarce in the peripheral subregions (e.g., Eastern Tien Shan, Eastern Himalaya,
26 and Hengduan Shan). The inventory ~~indicates~~further confirmed that surge activity is more likely to occur for ~~glaciers with~~
27 larger ~~and~~area, longer ~~glaciers~~length, and wider elevation range. ~~Among the glaciers with similar area, the surging ones usually~~
28 ~~have steeper slope than the non-surging ones.~~ Besides, we found a potential relationship between the ~~frequency of surge~~
29 ~~activities~~surging glacier concentration and regional glacier mass balance. The subregions with slightly negative or positive
30 mass balance hold large clusters of ~~surge-type~~surging glaciers, while those with severe glacier mass loss hold very few ~~surge-~~
31 ~~typesurging~~ glaciers. ~~In some subregions where glacier mass loss accelerated, the frequency of surge activities that occurred~~
32 ~~before 2000 was much higher than that after 2000.~~ The inventory is available at:
33 <https://doi.org/10.5281/zenodo.69449797486614> (Guo et al., 2022).

34 **Key words:** High Mountain Asia, ~~Surge-type~~Surging glacier inventory, elevation change, KH-9, Digital Elevation Model
35 (DEM)

36 1 Introduction

37 A surge is a glacier instability that translates into an abnormally fast flow over a period of a few months to years (Cogley et
38 al., 2011). A ~~surge-type~~surging glacier exhibits an active phase (surge) and a quiescent phase that may occur at quasi-periodic
39 intervals (Jiskoot, 2011). ~~Unlike the steady glacier flow that ice gradually moves downslope, the extreme active state of glacier~~

40 ~~surge is still an enigma. When~~While a glacier ~~surge occurs~~enters into the ~~surging states~~, a large volume of ice mass is
41 transported downstream at a higher-than-average speed. ~~In the quiescence phase, a glacier stores to the slow-moving status~~
42 ~~again, and after the surge, the deposited ice melts fast. Glacier surge can induce several kinds of hazards, e.g., glacier lake~~
43 ~~outbursts (GLOF) when proglacial lakes exist, mudslides when the glacier is on a narrow steep and moraine-based bed, or~~
44 ~~ice collapse when the glacier is already in a gravitational unsteady state. Such mountain hazards have been frequently reported~~
45 ~~in recent decades.~~
46 ~~gradually regains mass at upper recaches.~~Previous studies pointed out that the surge-type glaciers only occupy ~1% of total
47 glaciers (Jiskoot, 2011; Sevestre and Benn, 2015). However, glacier ~~surge is~~surges are far more than an occasional behavior
48 in some specific regions, such as the Alaska-Yukon (Clarke et al., 1986), Svalbard (Jiskoot et al., 2000; Farnsworth et al.,
49 2016), and Karakoram-Pamir (Bhambri et al., 2017; Goerlich et al., 2020; Guillet et al., 2022). ~~Accordingly, glacial hazards~~
50 ~~are frequent~~Glaciers in these regions ~~have experienced heterogeneous mass loss in the past decades~~ (Hugonnet et al., 2021)-
51 ~~A complete inventory of. How glacier surge-type glaciers inventory is a basis for the activities impact the glacier regional~~
52 ~~hazard assessment of mass balance needs further investigation, and to facilitate this kind of study, the glacier surges-~~ needed
53 ~~to be found out first.~~
54 ~~In recent years, substantial efforts have been made to access the internal governing rules of glacier surges, including the~~
55 ~~hydrological-control~~(Kamb, 1987; Fowler, 1987), ~~thermal-control~~(Fowler et al., 2001; Murray et al., 2003), ~~environmental~~
56 ~~factor~~(Hewitt, 2007; Van Wyk de Vries et al., 2022), ~~friction state~~(Thøgersen et al., 2019; Beaud et al., 2021), ~~and the unified~~
57 ~~enthalpy balance model~~ (Sevestre and Benn, 2015; Benn et al., 2019). ~~To support such studies, the accurate description of~~
58 ~~surging glacier distribution is needed to provide samples for studying the internal dynamic process of surges. Besides, Glacier~~
59 ~~surge can induce several kinds of hazards, e.g., glacier lake outbursts (GLOF)~~ (Round et al., 2017; Steiner et al., 2018),
60 ~~mudslides~~ (Muhammad et al., 2021), ~~or ice collapse~~ (Kääb et al., 2018; Paul, 2019). ~~Such mountain hazards have been~~
61 ~~frequently reported in recent decades~~ (Shugar et al., 2021; An et al., 2021; Kääb et al., 2021). ~~A complete inventory of surging~~
62 ~~glaciers is a basis for the regional hazard assessment of glacier surges.~~
63 Generally, a surging glacier ~~will~~could exhibit ~~four~~either one or several drastic changes, ~~including~~: extreme speed-up (by a
64 factor 10~1000 compared to normal conditions), distinct elevation change pattern, rapid terminus advance, and surface
65 ~~morphologi~~morphological changes (medial or looped moraine, crevasses, etc.) (Jiskoot, 2011). ~~Surge-type~~The identification
66 ~~of surging glaciers have been identified by many studies~~can be implemented based on the observation of the above changes,
67 e.g., glacier surface morphology (Clarke et al., 1986; Paul, 2015; Farnsworth et al., 2016), terminus position (Copland et al.,
68 2011; Vale et al., 2021), or glacier motion (Quincey et al., 2011). ~~As for the surge-type glacier, which refers to the glacier that~~
69 ~~possibly surged before, are generally identified by the indirect morphological evidence (without observed changes)~~ (Goerlich
70 et al., 2020). The visual interpretation of glacier surface ~~morphologi~~morphological changes is easy to operate, but fraught
71 with uncertainty due to the snow cover or the absence of supraglacial moraine (Jacquemart and Cicoira, 2022). To recognize
72 abnormal changes in glacier motion, a long-term flow velocity time series is needed (Yasuda and Furuya, 2015; Round et al.,
73 2017). Since the quiescent phase may last for decades and the image source for estimating the flow velocity is limited, the
74 abnormal changes in glacier motion are prone to be missed. ~~By contrast, the recognition of abnormal surface elevation changes~~
75 ~~is an effective way to identify the surging glaciers, which has been confirmed by several glacier mass-balance studies~~ (Bolch
76 et al., 2017; Zhou et al., 2018), ~~as its source datasets can satisfy the requirement of spatial-temporal coverage with~~
77 ~~comparatively fewer acquisitions.~~By combining observations of multiple features, the identification of ~~surge-type~~surging
78 glaciers could be more efficient and complete (Mukherjee et al., 2017; Goerlich et al., 2020; Guillet et al., 2022). However,
79 ~~the multi factor method is hard to be implemented~~when conducting such studies on a large spatial scale or a long temporal
80 scale ~~due to, one should select the least time-consuming but effective identification method. In that case, it's ideal to take the~~
81 ~~deficiency of data acquisitions. By contrast, the recognition of abnormal surface~~long-term elevation ~~changes is an effective~~
82 ~~way to identify the surge-type glaciers~~change as the criteria, ~~and to combine with other observations as complements if~~

83 ~~possible~~ (Guillet et al., 2022), ~~as its source datasets can satisfy the requirement of spatial-temporal coverage with comparatively~~
84 ~~fewer acquisitions.~~

85 Except for the polar regions, High Mountain Asia (HMA) is the most densely glacierized region in the world. Within the HMA
86 range, several subregions are famous for the concentration of ~~surge-typesurging~~ glaciers as well as the anomalous glacier mass
87 balance (Hewitt, 2005; Gardelle et al., 2013; Farinotti et al., 2020). The inventories of ~~surging or surge-type-like~~ glaciers have
88 been established for some subregions like the Karakoram (Bhambri et al., 2017), West-Kunlun (Yasuda and Furuya, 2015),
89 Pamir (Goerlich et al., 2020), Tien Shan (Mukherjee et al., 2017; Zhou et al., 2021). Sevestre and Benn (2015) presented the
90 first global ~~surge-typesurging~~ glacier inventory by reanalyzing historical reports from 1861 to 2013. However, it was compiled
91 from various data sources (publications, reports, etc.) with inconsistent spatial-temporal coverage, which makes it difficult to
92 ensure accuracy and completeness. Vale et al. (2021) identified 137 ~~surge-typesurging~~ glaciers across HMA by detecting
93 surge-induced terminus change and ~~morphologiemorphological~~ changes from Landsat images from 1987 to 2019. The number
94 is obviously underestimated, because it is smaller than the numbers of previous subregional inventories (Bhambri et al., 2017;
95 Goerlich et al., 2020). Guillet et al. (2022) presented a new ~~surge-typesurging~~ glacier inventory of HMA by identifying multiple
96 glacier change features. In total 666 ~~surge-typesurging~~ glaciers were identified across HMA. However, the glacier change
97 observation period is shorter than two decades (2000-2018), and therefore some ~~surge-typesurging~~ glaciers with relatively long
98 ~~revisit~~ cycles may be missed.

99 In this ~~paperstudy~~, we aimed to build a ~~new inventory to include more complete surge-typesurging glacier inventory~~
100 ~~aerosswithin~~ HMA based on glacier surface elevation change observations over four decades. A workflow was developed to
101 obtain the historical glacier surface elevation change from multiple datasets, including the KH-9 DEM (1970s), NASADEM
102 (2000), COP30 DSM (2011-2014), ~~and HMA8m DEM (2002-late 2016)~~, ~~and existed elevation change datasets~~. Glaciers in
103 the new inventory were divided into ~~fourthree~~ classes of confidence in surge detection. ~~After that, the elevation change based~~
104 ~~inventory were further complete and corrected by the long-term timeseries morphological feature identification~~ based on ~~the~~
105 ~~glacier elevation change pattern. Besides, the Landsat images (1986-2021). Based on the present inventory, the distribution~~
106 ~~and~~ geometric characteristics of ~~surge-typesurging~~ glaciers ~~within HMA~~ were ~~thoroughly~~statistically analyzed, ~~in order to~~
107 ~~clarify the factors affecting the glacier surge activity. demonstrate their spatial heterogeneity and geometrical difference from~~
108 ~~the normal glaciers.~~

109 2 Study region

110 High Mountain Asia consists of the Qinghai-Tibet Plateau and the surrounding regions, including the Karakoram, Pamir,
111 Himalayas, and Tien Shan. According to the ~~Randolphupdated~~ Glacier ~~Inventory version 6.0~~Area Mapping for Discharge from
112 ~~the Asian Mountains (GAMDAM2) glacier inventory~~, HMA hosts ~~95536131819~~ glaciers, covering a total area of
113 ~~~9760599817~~ km², ~~equal to 13.8% of the global glacier area~~ (Sakai, 2019). The Hindu Kush Himalayan Monitoring and
114 Assessment Programme (~~HiMAP~~) divided HMA into 22 subregions (Fig. 4) (Bolch et al., 2019). Different subregions are
115 influenced by different air currents, such as the South Asia monsoon, the East Asia monsoons, and the westerlies (Bolch et al.,
116 2012; Maussion et al., 2014). Glacier mass balance across HMA was found to be heterogeneous in the past decades (Gardelle
117 et al., 2013; Brun et al., 2017; Shean et al., 2020). In particular, glaciers in the Pamir-Karakoram-West Kunlun region had a
118 slightly positive or balanced mass budget (Hewitt, 2005; Zhou et al., 2017; Farinotti et al., 2020), while those in the Eastern
119 Himalayas, Nyainqentanglha and Hengduan Shan mountain ranges experienced substantial ice loss (Maurer et al., 2019).

120 3 Datasets

121 3.1 Elevation Data

122 The NASADEM is mainly reprocessed from the C-band SRTM (Shuttle Radar Topography Mission) images. Among the
123 current global DEMs, the NASADEM has the shortest source data acquisition period (~11/02/2000~22/02/2000) (Farr et al.,
124 2007). Based on an improved production flow, the NASADEM has a better performance than the earlier SRTM void-free
125 product in most regions (Crippen et al., 2016). The NASADEM was employed as the reference elevation source because its
126 acquisition time, 2000, is suitable to divide the elevation change observations to before and after 21st century with moderate
127 time span (one or two decades). Each tile of the product has an extent of $1^{\circ} \times 1^{\circ}$ and a pixel spacing of 1 arc-second (see Fig.
128 1a). In total 313 tiles were downloaded from NASA LP DAAC
129 (https://e4ftl01.cr.usgs.gov/MEASURES/NASADEM_HGT.001/).

130 Another global DEM we utilized is the newly released Copernicus DEM GLO-30-DGED (i.e., COP30 DEM). The COP30
131 DEM was edited from the delicate WorldDEM™, which was generated based on the TanDEM-X mission. The global RMSE
132 of COP30 DEM is ± 1.68 m (AIRBUS, 2020). Several studies have pointed out that this DEM is the most reliable open-access
133 DEM to date (Purinton and Bookhagen, 2021; Guth and Geoffroy, 2021). The source images of COP30 DEM were mostly
134 acquired between 2011 and 2014, and therefore COP30 DEM is suitable to represent the surface elevation in the 2010s. Like
135 the NASADEM, the COP30 DEM has a pixel spacing of 1 arc second. Each tile of product has an extent of $1^{\circ} \times 1^{\circ}$. In total
136 313 tiles were downloaded through ESA Panda (<https://panda.copernicus.eu/web/cds-catalogue/panda>).

137 The High Mountain Asia 8-meter DEM (HMA8m DEM) was also utilized in this study. The HMA8m DEM was generated
138 from high-resolution commercial optical satellite stereo images, including WorldView-1/2/3, GeoEye-1, and Quickbird-2
139 (Shean et al., 2020), through an automated photogrammetry workflow that is integrated with multiple error-control processes
140 (Shean et al., 2016). This DEM was originally produced for the mass balance estimation of HMA glaciers, so it covered most
141 of the glacierized regions in HMA. In total 3598 DEM tiles were downloaded from National Snow and Ice Data Center
142 (https://nsidc.org/data/HMA_DEM8m_MOS/versions/1). About 95% of them were acquired between 2010 and 2016 (Fig. 1b).
143 Due to the data voids and inconsistent acquisition time, the HMA8m DEM was taken as a supplementary elevation source to
144 increase the observations in the 2010s.

145 The Hexagon KeyHole-9 (KH-9) imagery was acquired in the 1970s. It is one of the earliest near-global satellite stereo image
146 source. The KH-9 imagery is characterized by a spatial resolution of 6-9 m, a wide coverage (130 km x 260 km), and a 70%
147 forward overlap (Surazakov and Aizen, 2010). Many studies have utilized this imagery to estimate historical glacier surface
148 elevation (Holzer et al., 2015; Zhou et al., 2017; Maurer et al., 2019). The KH-9 DEMs used in this study were generated
149 through the automated ASPy pipeline (Dehecq et al., 2020). The methodology, validated in the European Alps and Alaska
150 achieved a vertical accuracy of ~5m (68% confidence level). For more details on the method of KH-9 DEM generation, please
151 refer to Dehecq et al. (2020). In total 238 DEMs with a resolution of 48 m were generated from the KH-9 images acquired
152 between 1973 and 1980. The KH-9 DEMs were utilized to represent the glacier surface elevation in the 1970s (See Fig. 1c).

153 Several newly published elevation change datasets were also collected to include the most recent surges as much as possible
154 (Brun et al., 2017; Shean et al., 2020; Hugonnet et al., 2021). We mainly used the elevation change results presented by
155 Hugonnet et al. (2021) to extend the observation period to 2020, which has a resolution of 100 m and a temporal interval of 5
156 years. Through the inter-comparison of the multiple elevation change results, the gross errors or false signals in the elevation
157 change patterns could be easily detected.

158 3.2 Optical Satellite Images

159 In order to assist the identification of surging glacier, we also recognized the glacier morphological feature changes from multi-
160 temporal optical satellite images. The 1986-2021 Landsat imageries were mainly utilized to capture the glacier morphological

161 changes. We downloaded the false-colour composited Landsatlook images (geo-referenced) that have good brightness contrast
162 over snow/ice areas from USGS website (<https://earthexplorer.usgs.gov>). The images were pre-selected to satisfy the
163 requirement of cloud cover (<10%). In total, 7843 Landsatlook images in 148 frames were used (see Fig. 1d). We also utilized
164 the very high-resolution (VHR) images (Google/ESRI/Bing, etc.) as complements for surging feature identification. The fine
165 resolution of these images allows us to visually check the possible morphological features caused by past surges.

166 **3.3 Glacier inventory**

167 In this study, we used the GAMDAM2 glacier inventory (Sakai, 2019) as template for the surging glacier inventory, rather
168 than the Randolph Glacier Inventory V6.0 (RGI6.0) ~~outlines were utilized as templates for the surge type~~(RGI Consortium,
169 2017). The GAMDAM glacier inventory ~~has included many small glaciers that are missed in~~ RGI6.0, and provides ~~the spatially~~
170 more accurate glacier extent by excluding outcrop rocks and shaded areas (Nuimura et al., 2015) ~~and basic properties of~~. Since
171 the GAMDAM2 inventory only contains the glacier polygon vectors, we calculated the geometric and topographic attributes
172 for each glacier ~~with high level quality control in a way similar to that of RGI6.0~~. The maximum glacier centreline was
173 calculated through the Open Global Glacier Model (OGGM) (Maussion et al., 2019) ~~information in~~. The attributes ~~table~~
174 was/were used to interpret the geometric characteristics of ~~surge type~~surging glaciers.

175 **4 Methodology**

176 **4.1 Estimation of glacier surface elevation change**

177 The four kinds of DEMs have different coordinate references, vertical references, and data formats. Firstly, all DEMs were
178 converted to float GeoTiff format. For datasets with quality files (NASADEM and the COP30 DEM), the DEM were
179 preprocessed to mask out the pixels of low quality. The poor pixels of COP30 DEM tile were determined through the attached
180 height error map (with values larger than 2.5 m) and water body map (with values not equal to zero). The NASADEM was
181 directly masked with the attached water mask file. Subsequently, the coordinate system, map projection, and vertical reference
182 of all DEMs tiles were unified as the WGS84 coordinate system, HMA Albers Equal Area projection (Shean et al., 2020), and
183 WGS84 ellipsoid. The glacier surface elevation changes during 2000-2010s were derived by subtracting the NASADEM from
184 the COP30 DEM and HMA8m DEM, and those during 1970s-2000 were derived by subtracting the KH-9 DEM from the
185 NASADEM.

186 An automated DEM differencing workflow for large-scale glacier surface elevation change estimation was developed based
187 on the *demcoreg* package presented by Shean et al. (2019). The workflow integrated multiple DEM co-registration approaches,
188 the polynomial fit of tilt error, and other adaptive outlier removal approaches that was operated based on the observations over
189 stable regions. Hence, a mask that excluded the water bodies and glacierized regions was generated in advance. Before
190 differencing, the two DEMs need to be co-registered, because a small geolocation shift can result in considerable elevation
191 change errors in high mountain regions. The efficient analytical DEM co-registration method presented by Nuth and Kääb
192 (2011) was used to eliminate the relative geolocation shift between DEMs. This method assumes the geolocation shift vectors
193 of all DEM pixels are identical. However, for the global DEM products like NASADEM and COP30 DEM, a DEM tile was
194 usually mosaiced from multiple DEM patches, and the geolocation shift vectors at different parts of the DEM tile may be
195 different. In view of this problem, we developed a block-wise version of the analytical DEM co-registration method to reduce
196 the impacts of geolocation accuracy anisotropy of a DEM tile. Each DEM tile was divided into $m \times n$ blocks, and the DEM
197 shifts were estimated for each block. Then, the $m \times n$ groups of shift parameters were merged into one group of shift parameters
198 through a cubic interpolation. Technically, the estimated shift parameters become increasingly representative as the block size
199 decreases. However, the fitting of shift parameters requires a certain number of samples. The final block size was set to
200 300×300 pixels to reach the best balance between the representativeness and estimation accuracy of shift parameters. Besides,

201 we found that the block-wise co-registration method could result in wrong fitting of shift parameters over flat regions. To deal
202 with this, a threshold of mean slope (10°) was set to classify the DEMs into the flat and the hilly categories, and the original
203 global co-registration method (Nuth and Kääb, 2011) was applied to the flat ones.
204 Due to the residual orbital error of satellite images, the elevation difference maps often showed planimetric trends. This type
205 of systematic error was fitted as a universal surface trend using a quadratic polynomial model based on the observations in
206 stable regions, and then was removed from the elevation difference tile (Li et al., 2017). Besides, due to the jitter of the SAR
207 antenna and optical mapping camera, the elevation difference maps often showed stripes (i.e., band-like artifacts) (Yamazaki
208 et al., 2017). To eliminate the stripes, the elevation difference map was converted to the frequency domain through the Fast-
209 Fourier-Transform method. Since the cyclic values have a high frequency in the power spectral density map, a threshold of
210 frequency was set to separate the stripes components from the normal elevation differences. The de-stripping was completed
211 after the backward transformation. Finally, the outliers of elevation difference maps were reduced through the 3-sigma
212 threshold criteria.

213 The radar penetration into glacier surface can result in biases of elevation change estimation, which could be several to dozens
214 of meters, and potentially can lead to the false positive identification. We adopted a two-step procedure to reduce the radar
215 penetration bias in the final elevation change results. First, we used the DEM differencing workflow mentioned above to minus
216 the NASADEM from the SRTM-X DEM. The elevation differences over glacierized area were regarded as the penetration
217 difference between X-bands and C-bands. Secondly, we fitted a 3rd polynomial function between the glacial dH and altitude,
218 which was deemed as the penetration depth – altitude relationship. Then, the radar penetration biases were removed from the
219 COP30 DEM related results by taking the glacier elevation as input for the function. For the dH results calculated by
220 differencing NASADEM and optical DEMs (e.g. HMA8m and KH-9 DEM), the penetration difference of X- and C- bands
221 was multiplied by 2 to represent the absolute penetration depth of C-band (Abdel Jaber et al., 2019; Fan et al., 2022) and then
222 removed from the related results.

223 Finally, three elevation change maps were calculated: the COP30 DEM – NASADEM, the HMA8m DEM – NASADEM, and
224 the NASADEM – KH-9 DEM. The first two elevation change maps were ~~used~~combined with the three elevation change
225 datasets for the surge-type surging glacier identification during the period 2000-~~2010s~~2020, and the last one during the period
226 1970s-2000. In total, our elevation change observations covered ~92% of the total glacier area within HMA in 2000-~~2010s~~2020,
227 and ~77% in 1970s-2000. Gaps in observations were mainly due to: 1) data voids and incomplete coverage of original DEMs
228 tile, which was the main cause for the KH-9 DEMs and HMA8m DEM related results; 2) gross error removal during the
229 elevation change calculations, which led to the scattered holes in the COP30 DEM related results.

230 **4.3 Surge-type Surging glacier identification**

231 The identification of surging glaciers in this study were divided into three steps. First, we generated a raw inventory of surging
232 glaciers through the qualitative interpretation of multi-temporal elevation changes. Then, the visual identification of
233 morphological feature changes was carried out for the identified surging and surge-like glaciers. This procedure can further
234 confirm the surges or correct the false identifications based on glacier elevation changes (Guillet et al., 2022). The identified
235 results were re-checked by careful inspection on VHR images, and by comparing with existed surging glacier inventory. Also,
236 the surging tributaries were separated from the non-surging glacier trunk at this step.

237 **4.3.1 Identification through elevation changes**

238 In general, a typical glacier surge cycle can be divided into three phases (Jiskoot, 2011): 1) the build-up phase, characterized
239 by remarkable thickening in the upper reaches; 2) the active phase, characterized by remarkable thinning in the upper reaches
240 and thickening in the lower reaches; 3) the post-surge phase, characterized by strong down-wasting in the lower reaches. The
241 classical method of identifying surge-type surging glaciers is to recognize the combination of marked upper thinning and lower

242 thickening in the longitudinal direction. However, to distinguish the ~~surge-type~~surging glaciers in the build-up or post-surge
243 phase, careful comparison with surrounding glaciers is required. ~~It, which~~ is difficult to ~~identify a surge-type glacier in the~~
244 ~~build-up or post-surge phase~~be carried out with a mathematical index. ~~Moreover, multiple surge activities may occur at the~~
245 ~~tributaries of a large glacier system, especially in the Karakoram~~. In this study, we established a ~~four~~three-class indicator to
246 distinguish the surge possibility through the visual interpretation of glacier elevation change patterns:

- 247 I) ~~“verified”- either of 1)”:~~
248 ~~- a glacier having obviously thickened terminus (e.g. +30m); 2) a glacier having a combination of marked) obvious~~
249 ~~thickening in lower reaches (e.g. +30 m);~~
250 ~~- b) contrasting upper-thinning (e.g. -20m+20 m) and lower-thickening (e.g. +20m) in the longitudinal direction; 3)~~
251 ~~a glacier having a combination of marked+20 m);~~
252 ~~- c) contrasting upper-thickening (e.g. +20m+20 m) and lower-thinning (e.g. -30m)30 m);~~
253 ~~- d) severe thinning in the longitudinal direction-lower reaches (two time stronger than that of the normal glaciers,~~
254 ~~or comparable to the ablation of adjacent “verified” surging glaciers);~~
255 II) ~~“multiple”: a glacier having a “verified” surge type trunk and one or more “verified” surge type tributaries, or having~~
256 ~~two or more “verified” surge type tributaries.~~
257 III) ~~“II) “probable”: a glacier having a combination of”:~~
258 ~~- a) moderate upper thinning (e.g. -15m) and lower thickening (e.g. +15m) in the longitudinal direction while its~~
259 ~~neighbours have no such signals.+15m);~~
260 ~~IV)“- b) only moderate thickening in the middle reaches (e.g. +15m);~~
261 III) ~~“possible”- either of 1)”:~~
262 ~~- a glacier only having lower-) only moderate thickening at the terminus (e.g. +15m);~~
263 ~~- b) only strong thinning that is much in the lower reaches (one time stronger (e.g. two times) than the adjacent normal~~
264 ~~melting of surrounding glaciers (typically lower than -1 m/year); 2) a glacier only having upper thickening that is~~
265 ~~much more evident (e.g. two times) than surrounding glaciers (typically lower than +0.5 m/year).~~

266 Note that, the specific values of elevation change mentioned above were for information only. Because of the diversity in the
267 regional elevation change patterns under different climate or topographic conditions, the thresholds may vary spatially.

268 The identification of ~~surge-type~~surging glaciers was conducted separately ~~according to the~~in the two observation periods
269 ~~(1970s-2000 and 2000-2020). The sub-inventory covering the period 1970s-2000 was generated based on the dH results of~~
270 ~~NASADEM – KH-9 DEM. For the sub-inventory covering the period 2000-2020, its dH datasets contain the COP30 DEM –~~
271 ~~NASADEM, the HMA8m DEM – NASADEM, and three groups of previously published elevation change datasets (Brun et~~
272 ~~al., 2017; Shean et al., 2020; Hugonnet et al., 2021) observations. The sub-inventory based on the results of the NASADEM–~~
273 ~~KH-9 DEM was generated. Within each observation period, each glacier will be labelled with its possibility level of surging~~
274 ~~and elevation change pattern in the attribute table. For example, the label of “I-c” means this glacier was classified as “verified”~~
275 ~~surging glaciers because contrasting upper-thickening and lower-thinning pattern were observed in the corresponding period.~~
276 ~~Figure 2 shows an example of surging glacier identification result.~~

277 4.3.2 Identification through morphological feature changes

278 ~~Long-term Landsat images (acquired between 1986 and 2021) were utilized to represent the period of 1970s-2000. The two~~
279 ~~sub-inventories investigate the morphological change features of the three types of potential surging glaciers identified from~~
280 ~~elevation change. With each Landsat image acquisition frame, all Landsatlook images of different dates (acquired from 1986~~
281 ~~to 2021) were merged into an animated time-series image. Based on the COP30 DEM – NASADEM and the HMA8m DEM~~
282 ~~– NASADEM were generated animated image, we are able to easily identify the morphological feature changes. Regarding the~~
283 ~~moderate resolution of Landsat images, only three types of feature changes were utilized as criteria for identifying glacier~~

284 surges: terminus position change, looped moraine changes, and medial moraine changes. Similarly, we assigned a two-level
285 index to each morphological change to indicate our confidence at the identification, which was defined as follow:

286 1) terminus advance:

287 I) : obvious terminus advancing (e.g. over 500 m);

288 II): small terminus advancing (e.g. 0~500 m);

289 2) looped/medial moraine change:

290 I) : fast formation/vanishment of the looped moraine, or obvious distortion of the medial moraine;

291 II) : slow formation or vanishment of the looped moraine, or slight shape changes of existed looped moraine, or
292 slight distortion of the medial moraine.

293 Each of the three kinds of morphological changes were individually qualified and merged to representlabelled in the
294 periodattribute table.

295 4.3.3 Generation of 2000-2010s. For the final surging glacier inventory,

296 Through the above identification steps, in total five indicators were compiled to describe the changes of possible surging
297 glaciers. The two sub-inventories were merged together. The merging of sub-inventories of dH identified results were merge
298 firstly followed the principle of possibility. If a glacier was identified as a surge type glacier in one of two periods, it was
299 deemed as a surge type glacier in the final inventory., i.e., if a glacier was identified as a surge typesurging glacier in both
300 two periods but attached with different indicators, its indicator in the final inventory was taken from the indicator having a
301 higher possibility. The possibility of four types of indicators follows the order: ‘multiple’->“verified”->“”->“probable”->“”->
302 “possible”. For example, a glacier was identified as a multiple surge type“verified” surging glacier in the period of 1970s-
303 2000, and was identified as a probably surge type“probable” surging glacier in the period of 2000-2010s, then it was
304 deemedqualified as a ‘multiple’ surge type“verified” surging glacier in. After that, the merged dH indicators were further
305 compared with the morphological indicators to determine the final inventory. To ensure the consistency of the result, the work
306 of identifying surge type glaciersindicator of surge possibility. The “probable” or “possible” class was changed to a class with
307 higher possibility(e.g., from “probable” to “verified”) only if a “I” kind of morphological change was found.

308 We think the advancing glaciers usually have such features: 1) only thickened in a small area at terminus, without contrasting
309 upper thinning; 2) the advancing distance is relatively short (Lv et al., 2019, 2020; Goerlich et al., 2020)done by the same
310 person. Figure 2 shows an example of surge-. These features are corresponding to the “III-a” type glacier identification
311 resultsof elevation change, and “II” type of terminus advance. Therefore, if a glacier only shows these two kinds of changes,
312 it will be qualified as an advancing glacier, rather than a surging glacier.

313 For some glacier complexes that only tributary surged while the trunk did not, such as the Biafo glacier, Fedchenko Glacier
314 and Panmah Glacier (Hewitt, 2007; Goerlich et al., 2020; Bhambri et al., 2022), it’s necessary to separate the surging tributary
315 from the trunk. A tributary will be considered as an individual surging glacier if it has the following features. Firstly, the
316 dividing line of contrasting elevation change locates within this tributary. Secondly, the volume of mass contributed by this
317 tributary to the glacier trunk is relatively small. Then we manually edited the outline to separate the tributary from the glacier
318 complex. This kind of surges was also marked by the attribute of “trib_surge”.

319 In the final step, we inspected the identified surging glaciers on VHR imagery. The inspection aimed to remove the wrong
320 identification due to some false signals, such as the severe lower-thinning in a lake-terminated glacier and remarkable surface
321 heightening caused by nearby landslide. We also refined our inventory through the careful comparison with inventories
322 presented by Guillet et al. (2022), Goerlich et al. (2020) and Bhambri et al. (2017). For the surging glaciers that identified in
323 other inventories but not included in ours, we did a careful re-identification.

325 **5.1 ~~Surge-type~~Identified surging glaciers identification**

326 A total of ~~807 and 570~~1226 surge-type glaciers were identified during the periods of 2000-2010s and 1970s-2000, respectively.
 327 Due to the incomplete coverage and data voids of KH-9 DEMs, fewer surge-type glaciers were identified during the period of
 328 ~~1970s-2000. Finally, 1015~~related glaciers across the HMA were identified as surge-type glaciers (Fig. 3) based on the elevation
 329 ~~changes and morphological feature changes.~~ The identified surge-type~~related~~ glaciers consisted of ~~70 ‘multiple’ ones, 634~~890
 330 ‘verified’ ~~surging~~ ones, ~~196~~208 ‘probable’ ones, and ~~115~~128 ‘possible’ ones. ~~The area of ‘multiple’ and ‘verified’ surge-type~~
 331 ~~glaciers accounted for ~40% and ~43% of the~~ total surge-type of 175 surging tributaries were identified in 86 glacier area
 332 ~~(9112.97 km²), respectively.~~ complexes. When merging the identification results of the two periods, ~~36~~we found that a
 333 considerable proportion of identified surging glaciers were simultaneously recognized in two periods. This makes our
 334 inventory more convincing, since a surging glacier could exhibit different kinds of changes in different periods. For example,
 335 ~~26~~ probable and ~~125~~1 possible surge-type~~surging~~ glaciers identified during 2000-~~2010s~~2020 turned to be “‘verified’-surge-
 336 ~~type”~~ surging glaciers during 1970s-2000. Meanwhile, ~~45~~‘60 “probable” and ~~22~~‘21 “possible’-surge-type” surging glaciers
 337 identified during 1970s-2000 turned out to be ‘verified’ surge-type~~surging~~ glaciers during 2000-~~2010s~~2020. Thanks to an
 338 almost complete coverage of the elevation change observations, we were able to ~~an almost complete coverage of the elevation~~
 339 ~~change observations, we were able to~~ classify all glaciers in HMA. Table 1 shows the ~~detailed surge-type glacier identification~~
 340 ~~results~~ number of surging glaciers identified from two periods of elevation changes and morphological feature changes. Due to
 341 the incomplete coverage and data voids of KH-9 DEMs, fewer surging glaciers were identified during the period 1970s-2000.
 342 The “probable” and “possible” classes were deemed as surge-like glaciers. To avoid confusion, only the “verified” surging
 343 glaciers were used for analysis and comparison.

344 **5.2 Distribution of ~~surge-type~~surging glaciers**

345 ~~Surge-type~~Surging glaciers were identified in 21 subregions of HMA (except for the Dzhungarsky Alatau), however, the
 346 density of identified ~~surge-type~~surging glaciers is far from even (Fig. 3). ~~The surge-type glaciers~~Glacier surges are common
 347 in the northwest regions, sporadic in the inner regions, and scarce in the peripheral regions. Figure 4 and Table 2 show the
 348 ratios of ~~surge-type~~surging glacier number and area in each subregion. Considering the area of the smallest identified ~~surge-~~
 349 ~~typesurging~~ glacier is 0.~~3742~~ km², we only took the glaciers larger than 0.~~3040~~ km² in the glacier number related ratio. ~~The~~
 350 ~~surge-like glaciers were not accounted in such statistics.~~ The number (~~1015~~890) and area (~~22766.52~~16556.42 km²) of identified
 351 ~~surge-type~~surging glaciers accounted for ~2.49% and ~~~23.32~~16.59% of the total glacier number and glacier area in HMA,
 352 respectively.

353 Among the 22 subregions, the Karakoram is the largest cluster of ~~surge-type~~surging glaciers. In total ~~374~~354 surging and 128
 354 surge-type~~like~~ glaciers were identified in the Karakoram, ~~and 32 of them belonged to ‘multiple’ surge-type.~~ The number of
 355 ‘multiple’ surge-type~~and area of verified surging~~ glaciers in the Karakoram accounted for ~~45.73~~9.80% and ~~47.90~~% of HMA.
 356 Note that the ‘multiple’ surge-type glaciers are usually extra large glaciers (say 100 km² or larger). Hence, the area of surge-
 357 type glaciers ~~total glacier number and area within HMA.~~ In the Karakoram (~~11324.78~~ km²) is much larger than in other
 358 subregions, ~~surging glaciers has accounted for 8.59% of the total glacier number. We found more than half of the glacier area~~
 359 ~~tributary surges (101) in the Karakoram belongs to surge-type glaciers., where large glaciers are much more developed than~~
 360 ~~other regions. The area of surging glaciers occupied 39.48% of the total glacier area in Karakoram.~~ The Pamirs, composed of
 361 the Eastern Pamir, Western Pamir and Pamir Alay, hosts ~~282~~249 surging glaciers and 128 surge-type~~like~~ glaciers. About
 362 ~~33.82~~7.74% of the glacier area in the Eastern and Western Pamir ~~belong~~belongs to surge-type~~surging~~ glaciers. ~~Surge-type~~We
 363 also found 28 surging tributaries in 15 glacier complexes in the Pamirs. Surging glaciers are also common in the Western
 364 Kunlun. In total ~~96~~82 surging and 47 surge-type~~like~~ glaciers were identified in the West Kunlun, and ~~their~~the area of surging

365 glaciers accounted for 34.730.48% of the total glacier area. The Central Tien Shan has the fourth largest surge-typesurging
366 glacier area. In total 62surge-type59 surging glaciers were identified in the Central Tien Shan, which accounted for
367 49.5covered 12.93% of the total glacier area. The Karakoram, Pamirs, West Kunlun, and Central Tien Shan nourished ~8083%
368 of the surge-typesurging glaciers across HMA. Figure 5 shows the distribution of identified surging and surge-typelike glaciers
369 in these four regions.

370 Within interior HMA subregions (including the Tibetan Interior Mountains, Eastern Kunlun Shan, and Tanggula Shan), the
371 number of surge-typeidentified surging glaciers only covered aboutless than 2% of the total glacier number, but the area
372 accounted for about20near 15% of the total glacial area. Surge-typeSurging glaciers in these regions generally gathered in
373 some watersheds. Similar localized surge-typesurging glacier clusters were also found in the Nyainqentanglha, Northern and
374 Western Tien Shan, and Central Himalaya, but the corresponding area ratios are much lower. We also found ‘multiple’ surge-
375 type glaciers in the Western/Eastern Himalaya and Qilian Shan where surge events were rarely reported. In these regions, our
376 inventory covered dozens of surging glaciers which were rarely reported before. Figure 6 shows some samples of identified
377 surging glaciers in these regions.

378 5.3 Geometric characteristics of surge-typesurging glaciers

379 In this part, only the surging glaciers and non-surging- glaciers are taken for analysis. The surge-like glaciers are not included.
380 All glacier samples in the surging and non-surging classes are larger than 0.40 km².

381 We divided all glaciers larger than 0.30 km² into 119 classes according to their area, and calculated the ratios of surge-
382 typesurging glacier number and area in each class. Note that the smallest identified surge type glacier is 0.37 km². As shown
383 in Figure 6, surge-type7, surging glaciers were found in all classes. Both the ratios of surging glacier area and number became
384 increasingly high as the glacier size increased, except for the last class. Surging glaciers with an area of 1~50 km² occupies
385 82% of all surging glaciers. For the fourthree classes in which glaciers are larger than 50 km², the ratios of surge-typesurging
386 glaciers area and number were about 72.452% and 62.954%, respectively. For the two classes in which glaciers are larger than
387 300 km², the ratios of surge type glaciers area and number were over 85%. All the glaciers larger than 500 km² were identified
388 as ‘multiple’ surge-type glaciers. Fig. 6 shows that both the ratios of surge type glacier area and number became increasingly
389 high as the glacier class size increased, which indicated that the larger glaciers are more likely to be surge-type In particular,
390 2 of 6 very large glaciers-

391 We also analyzed the distribution of surge-type (the Siachen glacier number and Hispar glacier) surged during our
392 observation periods.

393 When comparing the geometric characteristics of the surging glaciers and non-surging glaciers, we selected samples in the
394 following way: for each surging glacier, we selected 10 non-surging glacier samples that have closest area in different aspects-;
395 and then we randomly sampled 3 out of the 10 selected non-surging glaciers. This is to minimize the discrepancy due to the
396 large gap resulted from the sample differences. There are two reasons for doing so. First, the gap between the sample numbers
397 is huge (~35000 non-surging vs. 890 surging). Second, a high proportion of non-surging glaciers are very small glaciers. The
398 final selected 890 × 3 non-surging glaciers formed the reference group.

399 We first analysed the distribution of surging glacier number and area in the sample sizes (~40000 vs. 1015), we randomly
400 sampled 1015 nonsurge type glaciers 1000 times, and calculated the distribution of sampled nonsurge type glaciers for each
401 time-eight orientations. As shown in Fig. 7, both the number and area of glaciers facing the north are the largest, and then
402 followed by those facing the northwest and northeast. In each aspect, The distribution of the standard deviations (STD) of
403 glacier numbers calculated from the 1000 repetitions of nonsurge type glacier samples is less orientation in reference group
404 were different than 1.4%, and the STD of glacier area is less than 3.8%, that of the non-surging glaciers, which means the
405 impact of the confirmed the statistical analysis would be affected by sample sizes on the glacier distribution is
406 negligible differences. The number of surge-typesurging glaciers facing the north accounted for ~3330.1% of the total surge-

407 ~~typesurging~~ glacier number, and their area accounted for ~~~28~~27.8% of all ~~surge-typesurging~~ glacier area. ~~In particular,~~The
408 number and area ratios of ~~surge-typesurging~~ glaciers facing the north are obviously higher than ~~that of~~ the non-~~surge-type~~
409 ~~glaciersurging glaciers~~ facing the north, while the number and area ratios of ~~surge-typesurging~~ glaciers facing the northwest
410 are obviously lower than ~~that of~~ the non-~~surge-type~~ ~~glaciernon-surgin~~ ~~glaciers~~ facing the northwest. ~~Meanwhile, the area ratio~~
411 ~~of surging glaciers facing the northeast is considerable higher than the number ratio, but for surging glaciers facing the~~
412 ~~northwest and southwest the situation is opposite.~~

413 Figure ~~8~~9 illustrates the comparisons between the basic geometric properties of ~~surge-type and nonsurge-type~~ ~~glaciers.~~ ~~As seen~~
414 ~~in figures 8a, 8b, and 8e, relative to nonsurge-type~~ ~~glaciers,~~ ~~surge-typesurging and non-surgin~~ ~~glaciers.~~ The sampling strategy
415 ~~mention above was also utilized here. If we directly compare the surging glaciers with all non-surgin~~ ~~glaciers, we will find~~
416 ~~that surging~~ glaciers generally have a larger area, wider elevation range (i.e., the highest glacier surface elevation minus the
417 lowest), and longer flowline. ~~The area of most surge-type glaciers is within the band of 3–50 km², and (Fig 9a-c). Taking the~~
418 ~~median value is 8.20 km², much larger than that of nonsurge-type glaciers (0.74 km²). The surface values as the candidates s,~~
419 ~~the quantitative comparisons are 7.3 km² (surging) vs. 0.87 km² (non-surgin) for glacier area, 1534 m vs. 642 m for elevation~~
420 ~~ranges of most surge-type glaciers are within the band of 1000–2500 m, and the median value is 1482 m, much higher than~~
421 ~~that of the nonsurge-type range, and 6695 m vs. 1854 m for maximum~~ glacier (574 m). ~~The discrepancey in the length between~~
422 ~~the two kinds of glaciers is even more evident. The median value of the length of surge-type glaciers is 6590 m, about 3.5~~
423 ~~times longer than that of the nonsurge-type glacier (1493 m), respectively.~~ In terms of mean surface slope and median elevation,
424 the values of the ~~surge-typesurging~~ glaciers are less spread out than the non-~~surge-type~~ ~~non-surgin~~ glaciers. However, the
425 median values of the two kinds of glaciers are very close (see Figures ~~8d and 8e~~) ~~9d and 9e~~). If we took the non-surgin glaciers
426 ~~in reference group for comparisons, the discrepancies of two kinds of groups on these geometric properties became much more~~
427 ~~different. The gaps between the surging and non-surgin glaciers (reference group) in the glacier area (7.3 km² vs. 7.0 km²),~~
428 ~~elevation range (1534 m vs. 1180 m) and glacier length (6695 m vs. 5560 m), are much smaller. More importantly, the mean~~
429 ~~slope of the glaciers in reference group become smaller than that of the surging glaciers.~~

430 The correlation between different glacier geometric properties was ~~analyzed~~analysed through the bivariate scatterplots (see
431 Figure ~~9~~10). Among the glacier area, glacier length, and glacier surface elevation range, any two of them have an apparent
432 positive correlation. The glacier mean slope has a moderate correlation with the glacier area, glacier length, and glacier
433 elevation range. By contrast, the glacier median elevation has little correlation with glacier area, glacier length, glacier
434 elevation range, and glacier mean slope. The correlation of any two geometric properties makes little difference between ~~surge-~~
435 ~~typesurging~~ and non-~~surge-type~~ ~~non-surgin~~ glaciers.

436 6 Discussion

437 6.1 Uncertainty analysis

438 The reliability of ~~surge-typesurging~~ glacier identification is directly related to the accuracy of glacier surface elevation change.
439 Assuming the uncertainties in surface elevation change are similar over glacierized areas and stable areas, we evaluated the
440 glacier elevation change uncertainties based on elevation change observations in stable areas, whose true values are zeros.
441 ~~Meanwhile, the uncertainties in the radar penetration calculation were also considered through the error propagation law.~~ The
442 normalized median absolute deviation (NMAD) is less sensitive to outliers and can be deemed as an alternative to standard
443 deviation (Höhle and Höhle, 2009). Hence, the NMAD was used to denote the uncertainty of individual glacier surface
444 elevation change tile (Li et al., 2017). Figure ~~10~~11 shows the NMAD of elevation change observations in stable areas within
445 each DEM differencing tile, which were used for the co-registration and biases removal during the glacier elevation change
446 estimation. Due to large distortions in the KH-9 images, the NASADEM - KH-9 DEM results had the highest uncertainties.
447 Benefiting from the advantages of bistatic SAR image pairs, the COP30 DEM has high quality, and the COP30 DEM related

448 results had the lowest uncertainties. The HMA8m DEM related results had moderate uncertainties. The average NMAD of all
449 DEM differencing tiles was smaller than 5 m. The significant elevation errors usually occurred in the highly rugged regions
450 such as crests and horns. The terrain of glacier surface is relatively gentle, and therefore the uncertainties of glacier surface
451 elevation changes should be lower than the estimated values. In general, the uncertainties of our elevation change results are
452 well-controlled. Compared with the typical surface elevation change resulted from a glacier surge (tens to hundreds of meters),
453 the magnitudes of uncertainties are very small.

454 Similar to previous studies (Sevestre and Benn, 2015; Goerlich et al., 2020), the ~~surge-type~~surging glacier identification in
455 this study was completed through a manual qualitative interpretation way. It's difficult to provide a quantitative index
456 to represent the uncertainty of surge identification. However, the four-class indicator of surge likelihood could aid that
457 in a degree.

458 6.2 Characteristics of ~~surge-type~~surging glaciers

459 The ~~comparison~~direct comparisons between geometric characteristics of ~~surge-type~~surging and ~~nonsurge-type~~non-surging
460 glaciers ~~manifests~~manifest that surge activity is more likely to occur in the glacier with a larger area, wider elevation range,
461 and longer length (Fig. 89). Previous studies also reported this phenomenon (Barrand and Murray, 2006; Jiskoot, 2011;
462 Sevestre and Benn, 2015; Mukherjee et al., 2017; Guillet et al., 2022). Larger area, wider elevation range, and longer length
463 mean a larger glacier scale and more mass storage. Surge is a self-balancing process of a glacier to regulate its internal
464 instability of thermal or hydrologic conditions which needs enough mass storage. In this case, about 97% of the surging glacier
465 has an area of larger than 1 km². For glaciers larger than ~~50~~10 km², surge becomes a quite common behavior; (with a number
466 ratio higher than 20%), rather than an accidental behavior (see Fig.67).

467 ~~Fig. 8d shows that,~~In terms of mean surface slope, ~~the values we could not observe a statistically difference in the median~~
468 ~~value of the surge-type surging and non-surging glaciers are,~~ although the surging glaciers have a more concentrated ~~than the~~
469 ~~nonsurge-type glaciers, but the median values of the two kinds of glaciers are very close (see Figures 8d and 8e).~~ Surge-type
470 ~~glaciers are larger value range (Fig 9d and tend to have a mean slope that is less spread than smaller glaciers (Figure 910, 3rd~~
471 ~~row, 1st column), which is the reason why).~~ After minimizing this kind of bias, we observed ~~a smaller spread for surge type~~
472 ~~glaciers on Figure 8d an obvious higher mean slope of surging glaciers in the comparison with the reference group. Several~~
473 ~~As shown in Fig. 9, among the nonsurge-type glaciers, the small ones occupy a high proportion and their mean slope presents~~
474 ~~strong randomness.~~ Previous studies have demonstrated that the ~~surge-type surging~~ glacier tend to have shallower slope (Jiskoot
475 et al., 2000; Guillet et al., 2022), ~~which is a consequence of.~~ However, here we reasonably argue that this rule was concluded
476 ~~from an unbalanced comparison, as the non-surging glaciers are consist of much larger proportion of small glaciers than surging~~
477 ~~glaciers does. Meanwhile,~~ the inverse relationship between the glacier slope and length (Clarke, 1991; Sevestre and Benn,
478 2015) ~~may not apply to very small glaciers (i.e. smaller than 1 km²).~~ ~~As shown in Fig.,~~ However, the rule that smaller glaciers
479 ~~have a higher mean slope does not apply to very small glaciers. If we set a threshold of glacier area (say 1 km²) when drawing~~
480 ~~Fig. 8d, the result could be different.~~9d and Fig. 10, among the non-surging glaciers, the small ones occupy a high proportion
481 ~~and their mean slope presents strong variability. Regarding this, we can conclude that steeper glaciers are more likely to surge~~
482 ~~when the comparison is restricted to similar areas. Considering the fact that steeper valley glaciers are more prone to reach the~~
483 ~~crucial gravitational imbalance, this conclusion should be reliable.~~ As for the glacier median elevation, since it is almost
484 irrelevant to the glacier area, glacier length, glacier elevation range, and glacier mean slope (see Fig. 910), it can be deemed
485 as an irregular glacier index. ~~However, among glaciers that have similar areas, steeper glaciers generally have lower median~~
486 ~~elevation. That's why the median elevation of surging glaciers is slightly smaller than that of non-surging glaciers (Fig. 9e).~~
487 ~~These comparisons could now lead to a conclusion as follows: the surging glaciers are generally longer, and have larger~~
488 ~~elevation spanning than non-leapfrog glaciers, since they have more mass storage. However, when glaciers are similar in area,~~
489 ~~a steeper surface slope is more likely to lead to surge.~~

490 Besides, our results manifested that the ratio distribution of ~~surge-type~~surging glaciers in eight aspects are slightly different
491 from that of ~~nonsurge-type~~non-surging glaciers (see Fig. 78). This is in line with the findings in previous studies (Bhambri et
492 al., 2017; Goerlich et al., 2020). In particular, the ratio of ~~surge-type~~surging glaciers is relatively higher than the non-~~surge~~
493 ~~typesurging~~ glaciers in the north direction, but lower in the northwest direction. This is mainly caused by the orientation of the
494 mountains in Karakoram and Pamir. It is generally known that glaciers facing the north are more developed in HMA. Due to
495 the orientation of the mountains, most of the large glaciers in Karakoram and Pamir flow toward the north and northeast. The
496 number of large glaciers flowing towards the northwest is much less. Accordingly, the ~~surge-type~~surging glaciers facing the
497 north and northeast are much more than that facing the northwest (see Fig. 5). The number of ~~surge-type~~surging glaciers in
498 Karakoram and Pamir accounts for a considerable proportion of the total number of ~~surge-type~~surging glaciers in HMA, and
499 therefore the orientation of ~~surge-type~~surging glaciers there has a great impact on the orientation distribution of ~~surge-~~
500 ~~typesurging~~ glaciers in HMA.

~~In the present inventory and analyses, we have not considered the impact of individual tributary surges. Multiple studies have
501 demonstrated that the tributary surge is an usual behavior within HMA. Hence, when surges only occur in the tributaries
502 within a glacier complex, biases could exist in the area-related analyses. The surge-related area could be overestimated.
503 Statistically speaking, a large mountain glacier is more likely to be classified as surge-type, due to the well-developed
504 tributaries. This could also help with the interpretation that larger glaciers are more likely to surge (Fig. 6), and surge-type
505 glaciers are more concentrated in the north direction (Fig. 7). Meanwhile, the frequent tributary surges may also lead to the
506 underestimation of surge-type glacier number, because surges occur in more than one tributary in a glacier complex
507 (correspond to the “multiple” surge-type class). However, the surging tributary is hard to separate from the glacier complex.
508 As the surging mass of a tributary injecting into the trunk, the surge-related area could expand beyond the extent of the tributary,
509 or occasionally, another surge in the glacier trunk could be activated.~~

511 The spatial distribution of ~~surge-type~~surging glaciers in HMA presents strong heterogeneity. About ~~8083~~% of identified ~~surge-~~
512 ~~typesurging~~ glaciers were located in the northwest region including the Central Tien Shan, Pamirs, Karakoram, and West
513 Kunlun, and their area occupied about ~~8687~~% of the total identified ~~surge-type~~surging glacier area (see Fig. 4 and Table 2).
514 As discussed above, larger glaciers are more likely to ~~be~~surge-type. The northwest regions generally hold more large glaciers,
515 and therefore hold more ~~surge-type~~surging glaciers. In other subregions, large glaciers are usually concentrated in some great
516 ice fields, such as the Geladandong, Puruogangri, and Xinqingfeng. Accordingly, ~~surge-type~~surging glaciers in these
517 subregions are usually clustered in several watersheds.

518 Several studies have pointed out that glacier surge activities have little impact on the glacier mass balance (Gardelle et al.,
519 2013; Bolch et al., 2017; Guillet et al., 2022). However, glacier mass balance may also affect the occurrence of glacier surge.
520 Copland et al. (2011) concluded that the increase of glacier surges in the Karakoram could be related to the positive mass
521 budget. The accumulated ice mass would accelerate a glacier to surge (Eisen et al., 2005; Kochtitzky et al., 2020), and the
522 significant mass loss could prevent or postpone the surge in return (Dowdeswell et al., 1995). On a regional large scale, the
523 relationship between mass balance and surge occurrence needs to be further ~~analyzed~~analysed. Our glacier elevation change
524 maps of the period 2000-2010s are similar to that derived by Brun et al. (2017) and Shean et al. (2020). We found that, at the
525 regional scale, the occurrence of ~~surge-type~~surging glaciers is correlated with the regional glacier mass balance. The three
526 subregions holding the largest clusters of ~~surge-type~~surging glaciers, i.e., the Pamirs, Karakoram, and West Kunlun, are
527 characterized by slightly negative or positive mass budgets, which is known as the ‘Pamir-Karakoram-West Kunlun’ anomaly
528 (Brun et al., 2017). Likewise, the subregions Central Tien Shan, Tibetan Interior Mountains, and East Kunlun Shan, which
529 hold the moderate clusters of ~~surge-type~~surging glaciers, have glacier mass loss rates much lower than the average rates of
530 HMA. By contrast, subregions with severe glacier mass loss hold the lowest ~~surge-type~~surging glacier ratio, such as the
531 Dzhungarsky Alatau, Hengduan Shan, and Eastern Himalaya.

532 Furthermore, we found that, in some subregions where glacier mass loss accelerated, the frequency of surge activities that
533 occurred before 2000 is much higher than that after 2000. For example, only 2 out of the 29 surge-type glaciers identified in
534 the Central Himalaya surged after 2000. In the Nyainqentanglha, all 16 surge-type glaciers were identified during the 1975s-
535 2000 period. Maurer et al. (2019) reported that glacier mass loss accelerated in the Central Himalaya during the past 40 years,
536 and Bhattacharya et al. (2021) reported that glacier mass loss accelerated in the Nyainqentanglha since 1960s. This could
537 indicate a positive relationship between the glacier surge frequency and glacier mass budget on the regional scale of HMA. A
538 glacier surge occurs when the gravitational potential energy exceeds a threshold, or the bottom water pressure exceeds a
539 threshold. Technically, glaciers undergoing severe mass loss have difficulties to accumulate enough mass to initiate the surge
540 activities. Also, the drainage system could be well established with the excessive and continuous meltwater input at the glacier
541 surface. This paper is focused on the surge-type glacier inventory in HMA. Further research is needed to corroborate whether
542 the observed and projected glacier mass loss will reduce the incidence of glacier surges in the future.

543 6.3 Comparison with previous ~~surge typesurging~~ glacier inventories

544 Guillet et al. (2022) presented a comprehensive ~~surge typesurging~~ glacier inventory of HMA for the period 2000-2018 from a
545 multi-factor remote sensing approach. ~~ThanksPrior to a longer observation periodthe comparison,~~ we ~~have identified more~~
546 ~~surge-type glaciers than~~ generated an inventory based on the RGI6.0, as Guillet et al. ~~in every subregion, especially in the~~
547 ~~Karakoram (374 vs. 223) and the Pamirs (282 vs. 223).~~ Within our inventory, 538 surge-type glaciers were also identified by
548 ~~Guillet et al. (2022) did(2022), i.e., 476 surge-type glaciers were newly identified in our study.~~ Guillet et al. (2022) identified
549 666 ~~surge typesurging~~ glaciers, and the area of ~~surge typesurging~~ glacier occupies 19.5% of the total glacier area. We identified
550 ~~4015 surge-type890 surging~~ glaciers, (809 if RGI6.0 was used), and their area only occupies ~~23.32~~16.59% of the total glacier
551 area. ~~Hence, most of~~ We attributed the ~~newly identified lower area ratio of surging~~ glaciers are small glaciers. ~~If considering~~
552 ~~only the period 2000-2010s for comparison,~~ to two reasons. First, in our inventory ~~the surging tributaries were separated from~~
553 ~~the non-surging trunks.~~ Second, many outcrop rocks and shaded areas are excluded from the GAMDAM2 glacier areas (Sakai,
554 2019), which would lower our surging area ratio, but make the result more accurate. If we assign our identified surging glaciers
555 to the RGI6.0 polygons without tributary separation, the surging area ratio would be larger (20.25%).
556 Within our inventory, 556 surging and 62 surge-like glaciers were ~~also documents more surge-type glaciers (807)~~
557 ~~than identified by Guillet et al. (2022).~~ Our results share 494 surge-type glaciers with ~~and the discrepancy of identifications~~
558 ~~mostly occurred on small glaciers.~~ If only the period 2000-2020 was considered, 657 surging glaciers were identified by us,
559 ~~which is very close to that of Guillet et al. (665).~~ For the period ~~of 1970s-2000,~~ there are 151 surging and 101 surge-like
560 ~~glaciers that were not identified by Guillet et al. (2022).~~ Overall, we have newly identified 231 surging and 248 surge-
561 ~~typelike~~ glaciers that were not included by Guillet's inventory. We owed the newly findings to the ~~much~~ longer observation
562 period and ~~the multi-level identification of the surge possibility (Guillet et al. only considered the "verified" type).~~ ~~multiple~~
563 ~~elevation change observation.~~ However, ~~128 surge-type glaciers identified~~ 47 surging glacier presented by Guillet et al. were
564 missed in this study, and 52 'probable' and 19 'possible' 62 surge-~~typelike~~ glaciers in our new inventory were identified as
565 'verified' ~~surge typesurging~~ glaciers by Guillet et al. (2022). ~~We carefully checked the glaciers not included in our inventory~~
566 ~~but included in Guillet et al's inventory, as well as those included in our inventory but not included in Guillet et al's inventory,~~
567 ~~and this step helped us to find 21 more surging glaciers.~~ We attribute this to the deficiency of using a single criterion, ~~because~~
568 ~~over the long observation period the elevation change signals caused~~ which could be aided by small-scale glacier surge activities
569 ~~may be diluted by the regular elevation changes~~ combining other features. Besides, the DEMs used in this study were suffering
570 from the data voids and incomplete spatial coverage, especially for the KH-9 DEM. ~~The earlier termination of our observation~~
571 ~~period (2014-2016 vs. 2018) could also partly explain the discrepancies,~~ which could result in a relatively conservative
572 identification.

573 Multiple studies have identified ~~surge-type~~surging glaciers in the Karakoram based on different data sources. For example,
574 Bhambri et al. (2017) identified 221 ~~surging and surge-type~~like glaciers (the tributaries of a glacier system are counted as
575 individual glaciers) based on the glacier morphology changes detected from ~~space-borne~~spaceborne optical images acquired
576 from 1972 to 2016, in-situ observations, and archive photos since the 1840s. ~~Also~~However, the boundary used by Bhambri et
577 al. (2017) to define the extent of Karakoram is much smaller than that used in our inventory. A much smaller group of ~~surge-~~
578 ~~typesurging~~ glaciers (88) were identified by Copland et al. (2011) based on a similar method and the data acquired between
579 1960 and 2013. Rankl et al. (2014) identified 101 ~~surge-type~~surging glaciers in the Karakoram by detecting the changes in
580 glacier surface velocity and terminus position between 1976 and 2012. The results of Guillet et al. (2022) should be more
581 reliable than previous ones, because more criteria were used for identifying ~~surge-type~~surging glaciers. Compared with
582 previous inventories, our inventory includes more surging glaciers (354). Among the 223 ~~surge-type~~surging glaciers in the
583 Karakoram identified by Guillet et al. (2022), ~~182 and 10 ones~~203 were identified as surging glaciers, and 12 were identified
584 as surge-like glaciers in this study, which means only 8 surging glaciers presented by us during the periods of 2000-2010s and
585 1970s-2000, respectively.Guillet et al. (2022) were not included in our inventory. The high coincidence between the two
586 inventories indicates our ~~surge-type~~surging glacier identification result is reliable. In total, we have newly identified 101
587 surging and 101 surge-like glaciers in this region.

588 In the Pamirs, Sevestre and Been (2015) identified 820 surge-type glaciers based on publications and reports, but Goerlich et
589 al. (2020) reported only ~~206 surge activities~~186 surging glaciers based on the observations of glacier flow velocity, elevation
590 change, etc.. We found that, if Goerlich et al. (2020) applied the GAMDAM2 glacier polygons used in this study, the number
591 of ~~surge activities~~identified by Goerlich et al. is in good agreement with that of Guillet et al. . Taking the RGI6.0 glacier
592 inventory as a reference, we found the identified 206 surges actually occurred in 176 RGI glacier complexes, surging glaciers
593 should be 182. Among the ~~176 surge type~~182 surging glaciers identified by Goerlich et al. (2020), ~~156~~153 and 15 were
594 ~~included in our inventory, identified as surging~~ and therefore ~~126~~surge-type-like glaciers in the Pamir were newly identified
595 our study, respectively. Although 14 surging glaciers are missed in this study, our inventory has contained other 94 surging
596 and 44 surge-like glaciers. The main cause for the result discrepancy is that the glacier elevation change observation conducted
597 by Goerlich et al. (2020) only covered parts of the Western Pamir and only the observations before 2000 were used. The
598 comparison demonstrated that 175 surge typeIn this region our inventory shared 193 surging glaciers with Guillet et al's
599 inventory, and 185 of them were identified by both this study (during the period 2000-2010s) and Guillet et al., 2020, which
600 also manifests a high coincidence of the two results.

601 In the West Kunlun, Yasuda and Furuya (2015) reported 9 ~~surge-type~~surging glaciers in the main range only, based on changes
602 in glacier flow velocity and terminus position of 31 glaciers, and other 9 ~~surge-type~~surging glaciers were found in the northwest
603 part of the West Kunlun Shan by Chudley et al. (2019). A ~~much~~ larger number (60) were found by Guillet et al. (2022).
604 However, our inventory has even included 96 more surging (82) and surge-typelike (47) glaciers in the West Kunlun Shan,
605 and 20 of them were identified. During the period ~~1970s-2000-2020,~~ we have identified 61 surging glaciers, which is very
606 close to the number presented by Guillet et al. (2022). In Central Tien Shan, Mukherjee et al. (2017) identified 39 surge-type
607 (9 surging and 30 surge-like) glaciers through the analysis of changes in surface elevation and morphology from 1964 to 2014,
608 whereas ~~62~~79 (59 surging and 20 surge-like) were identified in our studies. The insufficient coverage of elevation change
609 observation (only covered the west part of the Central Tien Shan) may be the main reason for the discrepancy in identification
610 results. Guillet et al. (2022) identified 54 ~~surge-type~~surging glaciers during 2000-2018, in which ~~37~~36 were confirmed in our
611 inventory.

612 7 Conclusions

613 This study presented a new inventory of ~~surge-type~~surging glaciers across the entire HMA range, which was accomplished
614 based on the glacier surface elevation changes derived from multiple elevation sources, by using the morphological feature
615 changes from optical images as complements. In total ~~1015~~890 surging and 336 surge-type-like glaciers were identified in the
616 new inventory. Through the analysis of geometric parameters, we found that ~~surge-type~~surging glaciers generally have a
617 greater area, length, and elevation range than ~~nonsurge-type~~non-surging glaciers. However, the differences are smaller than
618 we thought if taking the glacier size distribution into account. When glaciers having similar area, the steeper one is more likely
619 to surge. Furthermore, combining the region-wide glacier mass balance measurements, we found ~~that the frequency of surge~~
620 ~~occurrence decreased in several subregions that saw an accelerated~~a similar distribution between the positive mass loss balance
621 and number of surging glaciers. Benefiting from the long period and wide coverage of surface elevation change observations,
622 our study identified much more ~~surge-type~~surging glaciers in HMA than in previous studies. However, our inventory does not
623 provide the surge duration period and the maximum flow velocity to describe the dynamic process of each glacier surge activity.
624 Improvements should be made by combining multi-criteria identification methods. Considering the fact that ~~surge-type~~
625 ~~glaciers~~glacier surges are more widespread than we thought, the inventory presented in this study still needs further
626 replenishment.

627 8 Data and code availability

628 The presented inventory is freely available at: <https://doi.org/10.5281/zenodo.7486614> (Guo et al., 2022). The dataset is
629 composed of two files including the inventory itself and the associated metadata file. The inventory is distributed in the format
630 of GeoPackage ~~vector file~~ (.gpkg) and ESRI shpfile (.shp), which is represented by outline or centroid of surging glaciers
631 with geometric attributes. The glacier polygons, ~~geometric attributes~~ of the inventory are compiled from the RGI
632 v6.0-GAMDAM2 glacier inventory. In total ~~three~~eight fields are integrated in the attributes table to describe the surge
633 likelihoodsurging information of corresponding glacier ~~with the four class indicators~~as mentioned in section 4.3. The
634 description of each field in the attribute table is listed in Table 3. The metadata file is ~~distributed~~stored in the format of QGIS
635 ~~metadata~~a text file (~~qmd~~README.txt), which contains the description and details of the spatial/temporal attributes
636 information of the inventory.

637 The code used for elevation change estimation can be available at: https://github.com/TristanBlus/dem_coreg. This code was
638 developed based on the *demcoreg* package (Shean et al., 2019).

639 Author contribution

640 J.L. and L.G. conceived this study and wrote the paper. L.G. developed the processing flow, compiled the inventory and drew
641 the figures with the support from J.L. A.D. generated the KH-9 DEM. A.D., Z.L. and X.L. helped with the results analysis and
642 discussions and manuscript editing. Z.L., J.L. and J.Z. provided the funding acquisition. All authors have contributed and
643 agreed to the published version of the manuscript.

644 Competing interest

645 The authors declare that they have no conflict of interest.

646 Acknowledgments

647 The authors express gratitude to all institution that provide us the opensource dataset used in this study: the NASADEM from
648 LP DAAC (https://e4ftl01.cr.usgs.gov/MEASURES/NASADEM_HGT.001/), the Copernicus DEM from European Space
649 Agency (ESA) (<https://spacedata.copernicus.eu/web/cscda/cop-dem-faq>), the HMA8m DEM processed by David Shean from
650 National Snow and Ice Data Center (NSIDC) (https://nsidc.org/data/HMA_DEM8m_MOS/versions/1), and the Randolph
651 Glacier Inventory Version 6.0 (<http://www.glims.org/RGI/randolph.html>). The authors also appreciate the valuable comments
652 from Frank Pual and Guillet Gregoire.

653 Financial support

654 This work was supported by the Strategic Priority Research Program of Chinese Academy of Sciences (XDA20100101), the
655 National Natural Science Foundation of China (41904006), the National Natural Science Fund for Distinguished Young
656 Scholars (41925016), the Hunan Key Laboratory of remote sensing of ecological environment in Dongting Lake Area (No.
657 2021-010), the Fundamental Research Funds for the Central Universities of Central South University (2021zzts0265).

658 References

- 659 Abdel Jaber, W., Rott, H., Floricioiu, D., Wuite, J., and Miranda, N.: Heterogeneous spatial and temporal pattern of surface
660 elevation change and mass balance of the Patagonian ice fields between 2000 and 2016, *The Cryosphere*, 13, 2511–2535,
661 doi:10.5194/tc-13-2511-2019, 2019.
- 662 AIRBUS: Copernicus Digital Elevation Model Validation Report, AIRBUS Defence and Space GmbH, 2020.
- 663 An, B., Wang, W., Yang, W., Wu, G., Guo, Y., Zhu, H., Gao, Y., Bai, L., Zhang, F., Zeng, C., Wang, L., Zhou, J., Li, X., Li,
664 J., Zhao, Z., Chen, Y., Liu, J., Li, J., Wang, Z., Chen, W., and Yao, T.: Process, mechanisms, and early warning of glacier
665 collapse-induced river blocking disasters in the Yarlung Tsangpo Grand Canyon, southeastern Tibetan Plateau, *Sci. Total*
666 *Environ.*, 151652, doi:10.1016/j.scitotenv.2021.151652, 2021.
- 667 Barrand, N. E. and Murray, T.: Multivariate Controls on the Incidence of Glacier Surging in the Karakoram Himalaya, *Arct.*
668 *Antarct. Alp. Res.*, 38, 489–498, doi:10.1657/1523-0430(2006)38[489:MCOTIO]2.0.CO;2, 2006.
- 669 Beaud, F., Aati, S., Delaney, I., Adhikari, S., and Avouac, J.-P.: Generalized sliding law applied to the surge dynamics of
670 Shisper Glacier and constrained by timeseries correlation of optical satellite images, *Glaciers/Remote Sensing*, doi:10.5194/tc-
671 2021-96, 2021.
- 672 Benn, D. I., Fowler, A. C., Hewitt, I., and Sevestre, H.: A general theory of glacier surges, *J. Glaciol.*, 65, 701–716,
673 doi:10.1017/jog.2019.62, 2019.
- 674 Bhambri, R., Hewitt, K., Kawishwar, P., and Pratap, B.: Surge-type and surge-modified glaciers in the Karakoram, *Sci. Rep.*,
675 7, doi:10.1038/s41598-017-15473-8, 2017.
- 676 Bhambri, R., Hewitt, K., Haritashya, U. K., Chand, P., Kumar, A., Verma, A., Tiwari, S. K., and Rai, S. K.: Characteristics of
677 surge-type tributary glaciers, Karakoram, *Geomorphology*, 403, 108161, doi:10.1016/j.geomorph.2022.108161, 2022.
- 678 Bolch, T., Kulkarni, A., Kaab, A., Huggel, C., Paul, F., Cogley, J. G., Frey, H., Kargel, J. S., Fujita, K., Scheel, M., Bajracharya,
679 S., and Stoffel, M.: The State and Fate of Himalayan Glaciers, *Science*, 336, 310–314, doi:10.1126/science.1215828, 2012.
- 680 Bolch, T., Pieczonka, T., Mukherjee, K., and Shea, J.: Brief communication: Glaciers in the Hunza catchment (Karakoram)
681 have been nearly in balance since the 1970s, *The Cryosphere*, 11, 531–539, doi:10.5194/tc-11-531-2017, 2017.
- 682 Bolch, T., Shea, J. M., Liu, S., Azam, F. M., Gao, Y., Gruber, S., Immerzeel, W. W., Kulkarni, A., Li, H., Tahir, A. A., Zhang,
683 G., and Zhang, Y.: Status and Change of the Cryosphere in the Extended Hindu Kush Himalaya Region, in: *The Hindu Kush*

684 Himalaya Assessment, edited by: Wester, P., Mishra, A., Mukherji, A., and Shrestha, A. B., Springer International Publishing,
685 Cham, 209–255, doi:10.1007/978-3-319-92288-1_7, 2019.

686 Brun, F., Berthier, E., Wagnon, P., Kääb, A., and Treichler, D.: A spatially resolved estimate of High Mountain Asia glacier
687 mass balances from 2000 to 2016, *Nat. Geosci.*, 10, 668–673, doi:10.1038/ngeo2999, 2017.

688 Chudley, T. R. and Willis, I. C.: Glacier surges in the north-west West Kunlun Shan inferred from 1972 to 2017 Landsat
689 imagery, *J. Glaciol.*, 65, 1–12, doi:10.1017/jog.2018.94, 2019.

690 Clarke, G. K. C.: Length, width and slope influences on glacier surging, *J. Glaciol.*, 37, 236–246,
691 doi:10.3189/S0022143000007255, 1991.

692 Clarke, G. K. C., Schmok, J. P., Ommanney, C. S. L., and Collins, S. G.: Characteristics of surge-type glaciers, *J. Geophys.*
693 *Res. Solid Earth*, 91, 7165–7180, doi:10.1029/JB091iB07p07165, 1986.

694 Cogley, J. G., Arendt, A. A., Bauder, A., Braithwaite, R. J., Hock, R., J. B., R., Jansson, P., Kaser, G., Moller, M., Nicholson,
695 L., Rasmussen, L. A., and Zemp, M.: Glossary of glacier mass balance and related terms, IACS Contribution No.2, UNESCO,
696 Paris, 2011.

697 Copland, L., Sylvestre, T., Bishop, M. P., Shroder, J. F., Seong, Y. B., Owen, L. A., Bush, A., and Kamp, U.: Expanded and
698 Recently Increased Glacier Surging in the Karakoram, *Arct. Antarct. Alp. Res.*, 43, 503–516, 2011.

699 Crippen, R., Buckley, S., Agram, P., Belz, E., Gurrola, E., Hensley, S., Kobrick, M., Lavallo, M., Martin, J., Neumann, M.,
700 Nguyen, Q., Rosen, P., Shimada, J., Simard, M., and Tung, W.: NASADEM global elevation model: methods and progress,
701 *ISPRS - Int. Arch. Photogramm. Remote Sens. Spat. Inf. Sci.*, XLI-B4, 125–128, doi:10.5194/isprsarchives-XLI-B4-125-2016,
702 2016.

703 Dehecq, A., Gardner, A. S., Alexandrov, O., McMichael, S., Hugonnet, R., Shean, D., and Marty, M.: Automated Processing
704 of Declassified KH-9 Hexagon Satellite Images for Global Elevation Change Analysis Since the 1970s, *Front. Earth Sci.*, 8,
705 566802, doi:10.3389/feart.2020.566802, 2020.

706 Dowdeswell, J. A., Hodgkins, R., Nuttall, A.-M., Hagen, J. O., and Hamilton, G. S.: Mass balance change as a control on the
707 frequency and occurrence of glacier surges in Svalbard, Norwegian High Arctic, *Geophys. Res. Lett.*, 22, 2909–2912,
708 doi:10.1029/95GL02821, 1995.

709 Eisen, O., Harrison, W. D., Raymond, C. F., Echelmeyer, K. A., Bender, G. A., and Gorda, J. L. D.: Variegated Glacier, Alaska,
710 USA: a century of surges, *J. Glaciol.*, 51, 399–406, doi:10.3189/172756505781829250, 2005.

711 Fan, Y., Ke, C.-Q., Zhou, X., Shen, X., Yu, X., and Lhakpa, D.: Glacier mass-balance estimates over High Mountain Asia
712 from 2000 to 2021 based on ICESat-2 and NASADEM, *J. Glaciol.*, 1–13, doi:10.1017/jog.2022.78, 2022.

713 Farinotti, D., Immerzeel, W. W., Kok, R., Quincey, D. J., and Dehecq, A.: Manifestations and mechanisms of the Karakoram
714 glacier Anomaly, *Nat. Geosci.*, 13, 8–16, doi:10.1038/s41561-019-0513-5, 2020.

715 Farnsworth, W. R., Ingólfsson, Ó., Retelle, M., and Schomacker, A.: Over 400 previously undocumented Svalbard surge-type
716 glaciers identified, *Geomorphology*, 264, 52–60, doi:10.1016/j.geomorph.2016.03.025, 2016.

717 Farr, T. G., Rosen, P. A., Caro, E., Crippen, R., Duren, R., Hensley, S., Kobrick, M., Paller, M., Rodriguez, E., Roth, L., Seal,
718 D., Shaffer, S., Shimada, J., Umland, J., Werner, M., Oskin, M., Burbank, D., and Alsdorf, D.: The Shuttle Radar Topography
719 Mission, *Rev. Geophys.*, 45, RG2004, doi:10.1029/2005RG000183, 2007.

720 Fowler, A. C.: A theory of glacier surges, *J. Geophys. Res.*, 92, 9111, doi:10.1029/JB092iB09p09111, 1987.

721 Fowler, A. C., Murray, T., and Ng, F. S. L.: Thermally controlled glacier surging, *J. Glaciol.*, 47, 527–538,
722 doi:10.3189/172756501781831792, 2001.

723 Gardelle, J., Berthier, E., Arnaud, Y., and Kääb, A.: Region-wide glacier mass balances over the Pamir-Karakoram-Himalaya
724 during 1999–2011, *Cryosphere Discuss.*, 7, 975–1028, doi:10.5194/tcd-7-975-2013, 2013.

725 Goerlich, F., Bolch, T., and Paul, F.: More dynamic than expected: an updated survey of surging glaciers in the Pamir, *Earth*
726 *Syst. Sci. Data*, 12, 3161–3176, doi:10.5194/essd-12-3161-2020, 2020.

727 Guillet, G., King, O., Lv, M., Ghuffar, S., Benn, D., Quincey, D., and Bolch, T.: A regionally resolved inventory of High
728 Mountain Asia surge-type glaciers, derived from a multi-factor remote sensing approach, *The Cryosphere*, 16, 603–623,
729 doi:10.5194/tc-16-603-2022, 2022.

730 Guo, L., Li, J., Li, Z., Wu, L., Li, X., Hu, J., Li, H., Li, H., Miao, Z., and Li, Z.: The Surge of the Hispar Glacier, Central
731 Karakoram: SAR 3-D Flow Velocity Time Series and Thickness Changes, *J. Geophys. Res. Solid Earth*, 125,
732 doi:10.1029/2019JB018945, 2020.

733 Guth, P. L. and Geoffroy, T. M.: LiDAR point cloud and ICESat-2 evaluation of 1 second global digital elevation models:
734 Copernicus wins, *Trans. GIS*, 25, 2245–2261, doi:10.1111/tgis.12825, 2021.

735 Hewitt, K.: The Karakoram Anomaly? Glacier Expansion and the ‘Elevation Effect,’ *Karakoram Himalaya, Mt. Res. Dev.*, 25,
736 332–340, doi:10.1659/0276-4741(2005)025[0332:TKAGEA]2.0.CO;2, 2005.

737 Hewitt, K.: Tributary glacier surges: an exceptional concentration at Panmah Glacier, Karakoram Himalaya, *J. Glaciol.*, 53,
738 181–188, doi:10.3189/172756507782202829, 2007.

739 Höhle, J. and Höhle, M.: Accuracy assessment of digital elevation models by means of robust statistical methods, *ISPRS J.*
740 *Photogramm. Remote Sens.*, 64, 398–406, doi:10.1016/j.isprsjprs.2009.02.003, 2009.

741 Holzer, N., Vijay, S., Yao, T., Xu, B., Buchroithner, M., and Bolch, T.: Four decades of glacier variations at Muztagh Ata
742 (eastern Pamir): a multi-sensor study including Hexagon KH-9 and Pléiades data, *The Cryosphere*, 9, 2071–2088,
743 doi:10.5194/tc-9-2071-2015, 2015.

744 Hugonnet, R., McNabb, R., Berthier, E., Menounos, B., Nuth, C., Girod, L., Farinotti, D., Huss, M., Dussailant, I., Brun, F.,
745 and Kääb, A.: Accelerated global glacier mass loss in the early twenty-first century, *Nature*, 592, 726–731,
746 doi:10.1038/s41586-021-03436-z, 2021.

747 Jacquemart, M. and Cicoira, A.: Hazardous Glacier Instabilities: Ice Avalanches, Sudden Large-Volume Detachments of Low-
748 Angle Mountain Glaciers, and Glacier Surges, in: *Treatise on Geomorphology*, Elsevier, 330–345, doi:10.1016/B978-0-12-
749 818234-5.00188-7, 2022.

750 Jiskoot, H.: Glacier Surging, in: *Encyclopedia of Snow, Ice and Glaciers*, edited by: Singh, V. P., Singh, P., and Haritashya,
751 U. K., Springer Netherlands, Dordrecht, 415–428, doi:10.1007/978-90-481-2642-2_559, 2011.

752 Jiskoot, H., Murray, T., and Boyle, P.: Controls on the distribution of surge-type glaciers in Svalbard, *J. Glaciol.*, 46, 412–422,
753 doi:10.3189/172756500781833115, 2000.

754 Kääb, A., Leinss, S., Gilbert, A., Bühler, Y., Gascoin, S., Evans, S. G., Bartelt, P., Berthier, E., Brun, F., Chao, W.-A., Farinotti,
755 D., Gimbert, F., Guo, W., Huggel, C., Kargel, J. S., Leonard, G. J., Tian, L., Treichler, D., and Yao, T.: Massive collapse of
756 two glaciers in western Tibet in 2016 after surge-like instability, *Nat. Geosci.*, 11, 114–120, doi:10.1038/s41561-017-0039-7,
757 2018.

758 Kääb, A., Jacquemart, M., Gilbert, A., Leinss, S., Girod, L., Huggel, C., Falaschi, D., Ugalde, F., Petrakov, D., Chernomorets,
759 S., Dokukin, M., Paul, F., Gascoin, S., Berthier, E., and Kargel, J. S.: Sudden large-volume detachments of low-angle mountain
760 glaciers – more frequent than thought?, *The Cryosphere*, 15, 1751–1785, doi:10.5194/tc-15-1751-2021, 2021.

761 Kamb, B.: Glacier surge mechanism based on linked cavity configuration of the basal water conduit system, *J. Geophys. Res.*,
762 92, 9083, doi:10.1029/JB092iB09p09083, 1987.

763 Kochtitzky, W., Winski, D., McConnell, E., Kreutz, K., Campbell, S., Enderlin, E. M., Copland, L., Williamson, S., Main, B.,
764 and Jiskoot, H.: Climate and surging of Donjek Glacier, Yukon, Canada, *Arct. Antarct. Alp. Res.*, 52, 264–280,
765 doi:10.1080/15230430.2020.1744397, 2020.

766 Li, J., Li, Z., Zhu, J., Li, X., Xu, B., Wang, Q., Huang, C., and Hu, J.: Early 21st century glacier thickness changes in the
767 Central Tien Shan, *Remote Sens. Environ.*, 192, 12–29, doi:10.1016/j.rse.2017.02.003, 2017.

768 Lv, M., Guo, H., Lu, X., Liu, G., Yan, S., Ruan, Z., Ding, Y., and Quincey, D. J.: Characterizing the behaviour of surge- and
769 non-surge-type glaciers in the Kingata Mountains, eastern Pamir, from 1999 to 2016, *The Cryosphere*, 13, 219–236,
770 doi:10.5194/tc-13-219-2019, 2019.

771 Lv, M., Guo, H., Yan, J., Wu, K., Liu, G., Lu, X., Ruan, Z., and Yan, S.: Distinguishing Glaciers between Surging and
772 Advancing by Remote Sensing: A Case Study in the Eastern Karakoram, *Remote Sens.*, 12, 2297, doi:10.3390/rs12142297,
773 2020.

774 Maurer, J. M., Schaefer, J. M., Rupper, S., and Corley, A.: Acceleration of ice loss across the Himalayas over the past 40 years,
775 *Sci. Adv.*, 5, eaav7266, doi:10.1126/sciadv.aav7266, 2019.

776 Maussion, F., Scherer, D., Mölg, T., Collier, E., Curio, J., and Finkelnburg, R.: Precipitation Seasonality and Variability over
777 the Tibetan Plateau as Resolved by the High Asia Reanalysis, *J. Clim.*, 27, 1910–1927, doi:10.1175/JCLI-D-13-00282.1, 2014.

778 Maussion, F., Butenko, A., Champollion, N., Dusch, M., Eis, J., Fourteau, K., Gregor, P., Jarosch, A. H., Landmann, J.,
779 Oesterle, F., Recinos, B., Rothenpieler, T., Vlug, A., Wild, C. T., and Marzeion, B.: The Open Global Glacier Model (OGGM)
780 v1.1, *Geosci. Model Dev.*, 12, 909–931, doi:10.5194/gmd-12-909-2019, 2019.

781 Muhammad, S., Li, J., Steiner, J. F., Shrestha, F., Shah, G. M., Berthier, E., Guo, L., Wu, L., and Tian, L.: A holistic view of
782 Shisper Glacier surge and outburst floods: from physical processes to downstream impacts, *Geomat. Nat. Hazards Risk*, 12,
783 2755–2775, doi:10.1080/19475705.2021.1975833, 2021.

784 Mukherjee, K., Bolch, T., Goerlich, F., Kutuzov, S., Osmonov, A., Pieczonka, T., and Shesterova, I.: Surge-Type Glaciers in
785 the Tien Shan (Central Asia), *Arct. Antarct. Alp. Res.*, 49, 147–171, doi:10.1657/AAAR0016-021, 2017.

786 Murray, T., Strozzi, T., Luckman, A., Jiskoot, H., and Christakos, P.: Is there a single surge mechanism? Contrasts in dynamics
787 between glacier surges in Svalbard and other regions: IS THERE A SINGLE SURGE MECHANISM?, *J. Geophys. Res. Solid*
788 *Earth*, 108, doi:10.1029/2002JB001906, 2003.

789 Nuimura, T., Sakai, A., Taniguchi, K., Nagai, H., Lamsal, D., Tsutaki, S., Kozawa, A., Hoshina, Y., Takenaka, S., Omiya, S.,
790 Tsunematsu, K., Tshering, P., and Fujita, K.: The GAMDAM glacier inventory: a quality-controlled inventory of Asian
791 glaciers, *The Cryosphere*, 9, 849–864, doi:10.5194/tc-9-849-2015, 2015.

792 Nuth, C. and Kääb, A.: Co-registration and bias corrections of satellite elevation data sets for quantifying glacier thickness
793 change, *The Cryosphere*, 5, 271–290, doi:10.5194/tc-5-271-2011, 2011.

794 Paul, F.: Revealing glacier flow and surge dynamics from animated satellite image sequences: examples from the Karakoram,
795 *The Cryosphere*, 9, 2201–2214, doi:10.5194/tc-9-2201-2015, 2015.

796 Paul, F.: Repeat Glacier Collapses and Surges in the Amney Machen Mountain Range, Tibet, Possibly Triggered by a
797 Developing Rock-Slope Instability, *Remote Sens.*, 11, 708, doi:10.3390/rs11060708, 2019.

798 Pfeffer, W. T., Arendt, A. A., Bliss, A., Bolch, T., Cogley, J. G., Gardner, A. S., Hagen, J.-O., Hock, R., Kaser, G., Kienholz,
799 C., Miles, E. S., Moholdt, G., Mölg, N., Paul, F., Radić, V., Rastner, P., Raup, B. H., Rich, J., Sharp, M. J., and The Randolph
800 Consortium: The Randolph Glacier Inventory: a globally complete inventory of glaciers, *J. Glaciol.*, 60, 537–552,
801 doi:10.3189/2014JoG13J176, 2014.

802 Purinton, B. and Bookhagen, B.: Beyond Vertical Point Accuracy: Assessing Inter-pixel Consistency in 30 m Global DEMs
803 for the Arid Central Andes, *Front. Earth Sci.*, 9, 758606, doi:10.3389/feart.2021.758606, 2021.

804 Quincey, D. J., Braun, M., Glasser, N. F., Bishop, M. P., Hewitt, K., and Luckman, A.: Karakoram glacier surge dynamics,
805 *Geophys. Res. Lett.*, 38, n/a-n/a, doi:10.1029/2011GL049004, 2011.

806 Rankl, M., Kienholz, C., and Braun, M.: Glacier changes in the Karakoram region mapped by multitemporal satellite imagery,
807 *The Cryosphere*, 8, 977–989, doi:10.5194/tc-8-977-2014, 2014.

808 RGI Consortium: Randolph Glacier Inventory - A Dataset of Global Glacier Outlines, Version 6, doi:10.7265/4M1F-GD79,
809 2017.

810 Round, V., Leinss, S., Huss, M., Haemmig, C., and Hajnsek, I.: Surge dynamics and lake outbursts of Kyagar Glacier,
811 Karakoram, *The Cryosphere*, 11, 723–739, doi:10.5194/tc-11-723-2017, 2017.

812 Sakai, A.: Brief communication: Updated GAMDAM glacier inventory over high-mountain Asia, *The Cryosphere*, 13, 2043–
813 2049, doi:10.5194/tc-13-2043-2019, 2019.

814 Sevestre, H. and Benn, D. I.: Climatic and geometric controls on the global distribution of surge-type glaciers: implications
815 for a unifying model of surging, *J. Glaciol.*, 61, 646–662, doi:10.3189/2015JoG14J136, 2015.

816 Shean, D., Shashank Bhushan, Lilien, D., and Meyer, J.: dshean/demcoreg: Zenodo DOI release, ,
817 doi:10.5281/ZENODO.3243481, 2019.

818 Shean, D. E., Alexandrov, O., Moratto, Z. M., Smith, B. E., Joughin, I. R., Porter, C., and Morin, P.: An automated, open-
819 source pipeline for mass production of digital elevation models (DEMs) from very-high-resolution commercial stereo satellite
820 imagery, *ISPRS J. Photogramm. Remote Sens.*, 116, 101–117, doi:10.1016/j.isprsjprs.2016.03.012, 2016.

821 Shean, D. E., Bhushan, S., Montesano, P., Rounce, D. R., Arendt, A., and Osmanoglu, B.: A Systematic, Regional Assessment
822 of High Mountain Asia Glacier Mass Balance, *Front. Earth Sci.*, 7, 363, doi:10.3389/feart.2019.00363, 2020.

823 Shugar, D. H., Jacquemart, M., Shean, D., Bhushan, S., Upadhyay, K., Sattar, A., Schwanghart, W., McBride, S., de Vries, M.
824 V. W., Mergili, M., Emmer, A., Deschamps-Berger, C., McDonnell, M., Bhambri, R., Allen, S., Berthier, E., Carrivick, J. L.,
825 Clague, J. J., Dokukin, M., Dunning, S. A., Frey, H., Gascoïn, S., Haritashya, U. K., Huggel, C., Käab, A., Kargel, J. S.,
826 Kavanaugh, J. L., Lacroix, P., Petley, D., Rupper, S., Azam, M. F., Cook, S. J., Dimri, A. P., Eriksson, M., Farinotti, D., Fiddes,
827 J., Gnyawali, K. R., Harrison, S., Jha, M., Koppes, M., Kumar, A., Leinss, S., Majeed, U., Mal, S., Muhuri, A., Noetzli, J.,
828 Paul, F., Rashid, I., Sain, K., Steiner, J., Ugalde, F., Watson, C. S., and Westoby, M. J.: A massive rock and ice avalanche
829 caused the 2021 disaster at Chamoli, Indian Himalaya, *Science*, 373, 300–306, doi:10.1126/science.abh4455, 2021.

830 Steiner, J. F., Kraaijenbrink, P. D. A., Jiduc, S. G., and Immerzeel, W. W.: Brief communication: The Khurdopin glacier surge
831 revisited – extreme flow velocities and formation of a dammed lake in 2017, *The Cryosphere*, 12, 95–101, doi:10.5194/tc-12-
832 95-2018, 2018.

833 Surazakov, A. and Aizen, V.: Positional Accuracy Evaluation of Declassified Hexagon KH-9 Mapping Camera Imagery,
834 *Photogramm. Eng. Remote Sens.*, 76, 603–608, doi:10.14358/PERS.76.5.603, 2010.

835 Thøgersen, K., Gilbert, A., Schuler, T. V., and Malthe-Sørenssen, A.: Rate-and-state friction explains glacier surge propagation,
836 *Nat. Commun.*, 10, 2823, doi:10.1038/s41467-019-10506-4, 2019.

837 Vale, A. B., Arnold, N. S., Rees, W. G., and Lea, J. M.: Remote Detection of Surge-Related Glacier Terminus Change across
838 High Mountain Asia, *Remote Sens.*, 13, 1309, doi:10.3390/rs13071309, 2021.

839 Van Wyk de Vries, M., Wickert, A. D., MacGregor, K. R., Rada, C., and Willis, M. J.: Atypical landslide induces speedup,
840 advance, and long-term slowdown of a tidewater glacier, *Geology*, doi:10.1130/G49854.1, 2022.

841 Yamazaki, D., Ikeshima, D., Tawatari, R., Yamaguchi, T., O’Loughlin, F., Neal, J. C., Sampson, C. C., Kanae, S., and Bates,
842 P. D.: A high-accuracy map of global terrain elevations, *Geophys. Res. Lett.*, 44, 5844–5853, doi:10.1002/2017GL072874,
843 2017.

844 Yasuda, T. and Furuya, M.: Dynamics of surge-type glaciers in West Kunlun Shan, Northwestern Tibet: SURGE-TYPE
845 GLACIERS IN WEST KUNLUN SHAN, *J. Geophys. Res. Earth Surf.*, 120, 2393–2405, doi:10.1002/2015JF003511, 2015.

846 Zhou, S., Yao, X., Zhang, D., Zhang, Y., Liu, S., and Min, Y.: Remote Sensing Monitoring of Advancing and Surging Glaciers
847 in the Tien Shan, 1990–2019, *Remote Sens.*, 13, 1973, doi:10.3390/rs13101973, 2021.

848 Zhou, Y., Li, Z., and Li, J.: Slight glacier mass loss in the Karakoram region during the 1970s to 2000 revealed by KH-9
849 images and SRTM DEM, *J. Glaciol.*, 63, 331–342, doi:10.1017/jog.2016.142, 2017.

850 Zhou, Y., Li, Z., Li, J., Zhao, R., and Ding, X.: Glacier mass balance in the Qinghai–Tibet Plateau and its surroundings from
851 the mid-1970s to 2000 based on Hexagon KH-9 and SRTM DEMs, *Remote Sens. Environ.*, 210, 96–112,
852 doi:10.1016/j.rse.2018.03.020, 2018.

854 Table 1: ~~Surge-type~~Surging glacier identification results

Glacier changes	Identification class			Total
	I	II	III	
2000-2020 elevation change	719	157	169	1045
1970s-2000 elevation change	507	156	57	720
1986-2021 terminus advance	247	397	-	645
1986-2021 looped moraine	112	31	-	144
1986-2021 medial moraine	69	29	-	108
Final identified surging glaciers	890 (verified)	208 (probable)	128 (possible)	1226

855 * The identified surge type glaciers in 2000-2010s and 1970s-2000 partly coincide with each other.

856

857 Table 2: Results of ~~surge-type~~surging glacier identification in 22 subregions of HMA. Only glaciers larger than 0.34 km² were considered in the glacier number related values.

858

HiMAP regions	Glacier Number				Glacier Area			
	Surging	Surge-like	Total	Ratio (%)	Surging	Surge-like	Total	Ratio (%)
Karakoram	354	128	4121	8.59	7936.12	1329.40	20103.68	39.48
Western Pamir	188	48	3058	6.15	2232.52	289.597	8172.64	27.32
Western Kunlun Shan	82	47	2508	3.27	2580.21	589.17	8466.12	30.48
Central Tien Shan	59	20	2248	2.62	881.61	305.47	6816.95	12.93
Eastern Pamir	56	16	1148	4.88	796.35	79.12	2746.47	29.00
Tanggula Shan	22	4	697	3.16	441.94	41.71	1937.39	22.81
Tibetan Interior Mountains	22	12	1471	1.50	286.29	140.22	3933.48	7.28
Northern Western Tien Shan	21	6	1374	1.53	116.27	81.09	2502.60	4.65
Central Himalaya	17	21	3433	0.50	164.12	185.07	9928.72	1.65
Eastern Kunlun Shan	16	7	1191	1.34	458.11	55.38	2960.26	15.48
Nyainqentanglha	10	5	2916	0.34	119.53	184.79	7216.62	1.66
Eastern Hindu Kush	9	5	1279	0.70	178.18	77.19	3055.80	5.83
Western Himalaya	9	4	3659	0.25	110.22	69.41	8619.19	1.28
Eastern Himalaya	6	0	1334	0.45	94	0	3371.89	2.79
Pamir Alay	5	0	991	0.50	35.72	0	1957.94	1.82
Qilian Shan	4	6	851	0.47	35.99	26.40	1627.94	2.21
Eastern Tibetan Mountains	3	2	156	1.92	36.33	3.85	341.46	10.64
Altun Shan	2	3	156	1.28	4.13	3.17	294.95	1.40
Eastern Tien Shan	2	1	1243	0.16	12.03	2.59	2440.11	0.49
Hengduan Shan	2	0	700	0.29	26.22	0	1335.39	1.96
Gangdise Mountains	1	0	768	0.13	10.52	0	1339.54	0.79
Dzhungarsky Alatau	0	1	407	0	0	10.98	648.61	0
Total	890	336	35709	2.49	16556.42	3474.60	99817.72	16.59

859 * The value of ratio only considered the number and area of surging glaciers.

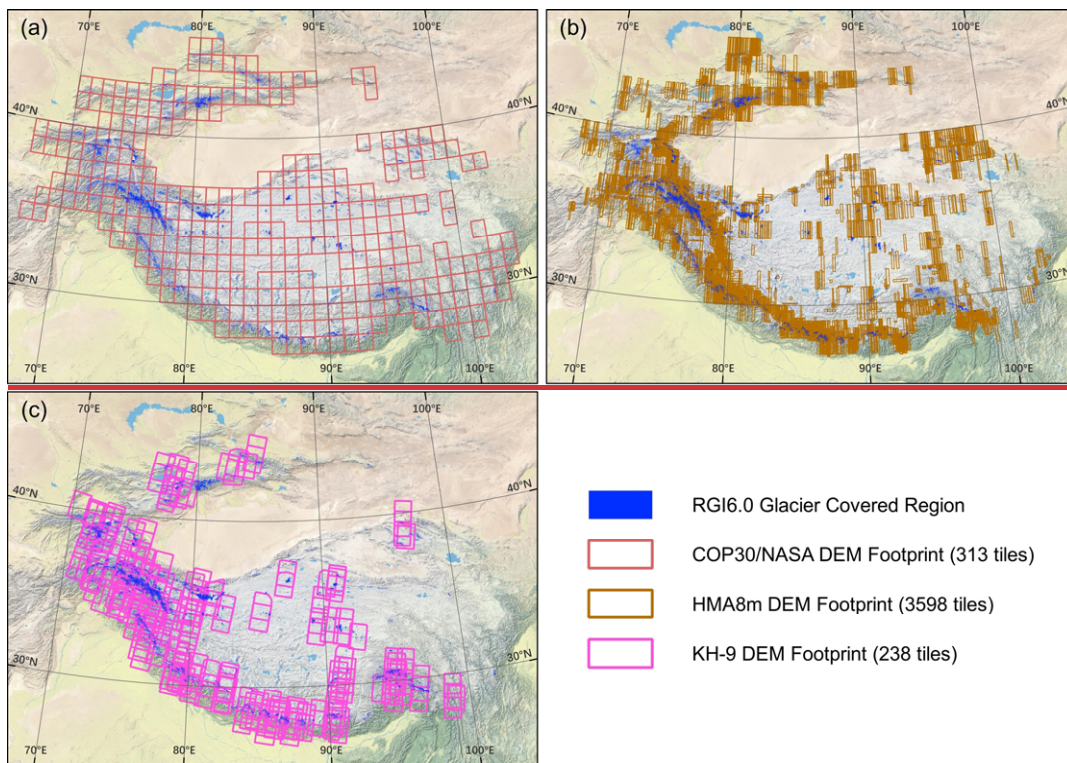
860

861 Table 3: Attribute information in the present ~~surge-type~~surging glacier inventory.

Attribute	Description	Attribute	Description
Glac_ID	Glacier identifier composed by Lat/Lon	Surge_20	Surge identified in 2000-2020 by dH
Area	Glacier covered area (km ²)	Surge_70s	Surge identified in 2000-2020 by dH
Zmin	Minimum elevation of the glacier (m a.s.l)	Delta_T	Identified class of glacier terminus advance

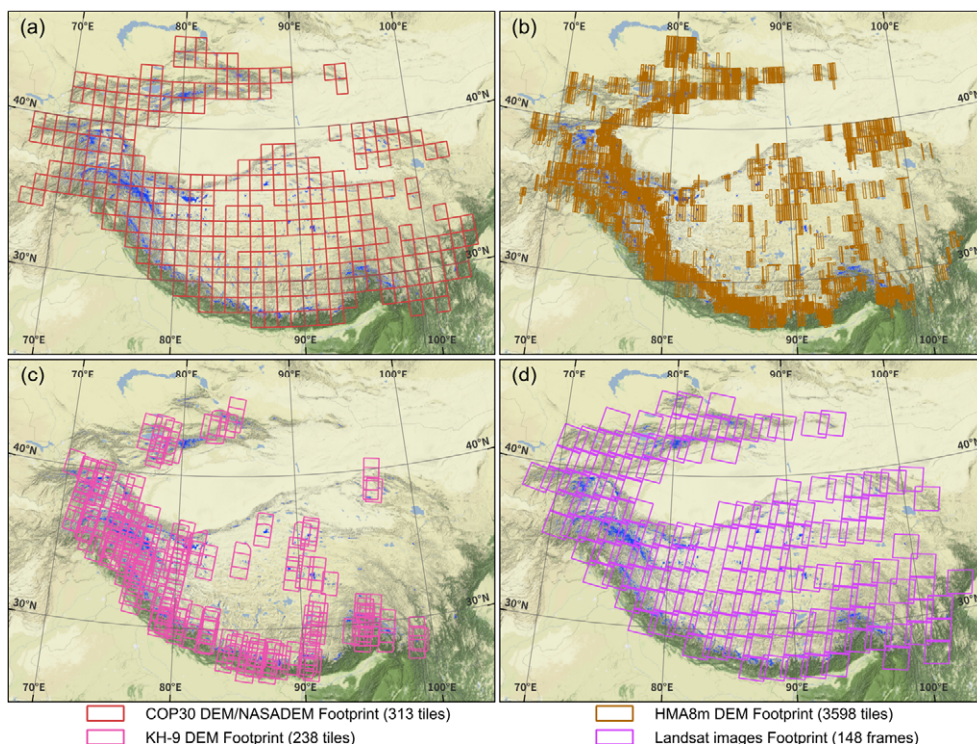
Zmax	Maximum elevation of the glacier (m a.s.l)	Loop_M	Identified class of looped moraine change
Zmed	Median elevation of the glacier (m a.s.l)	Medial_M	Identified class of medial moraine change
Slope	Mean glacier mean surface slope (°)	False_signal	False positive signal of identification
Aspect	Mean glacier aspect/orientation (°)	Trib_surge	If the glacier has/is surging tributary
MaxL	Maximum length of glacier flow line (m)	Surge_class	Final surge identification during 1970s-2020
HiMAP_region	HMA subregion that the glacier belongs to		

862



863

864

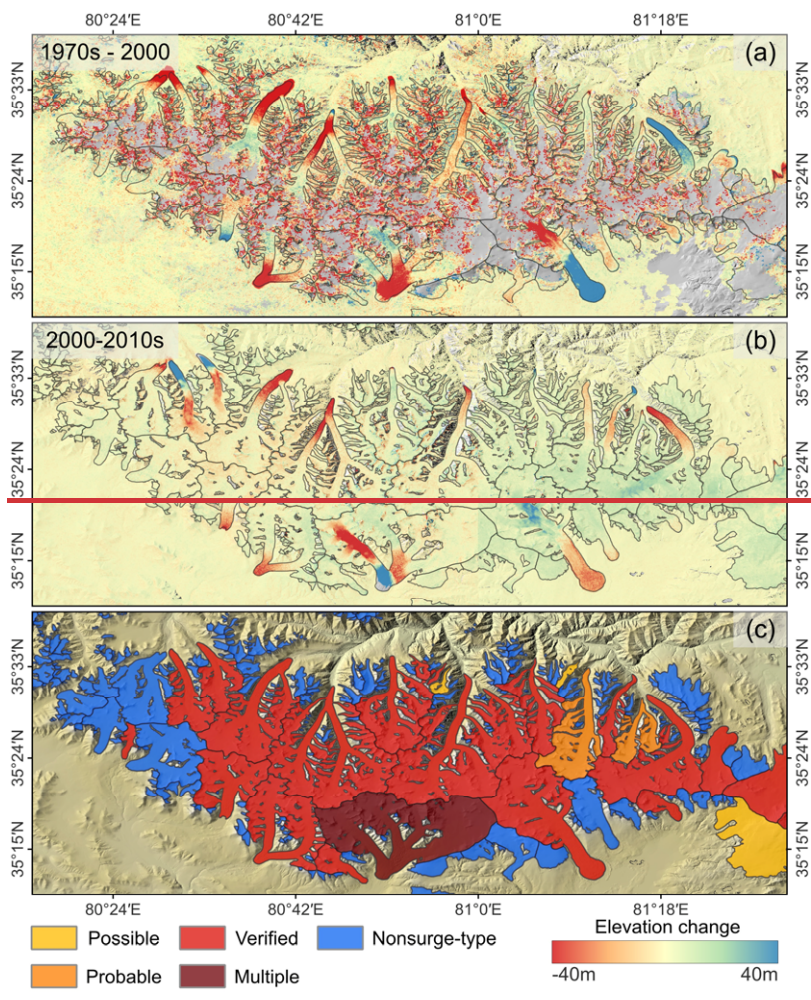


865

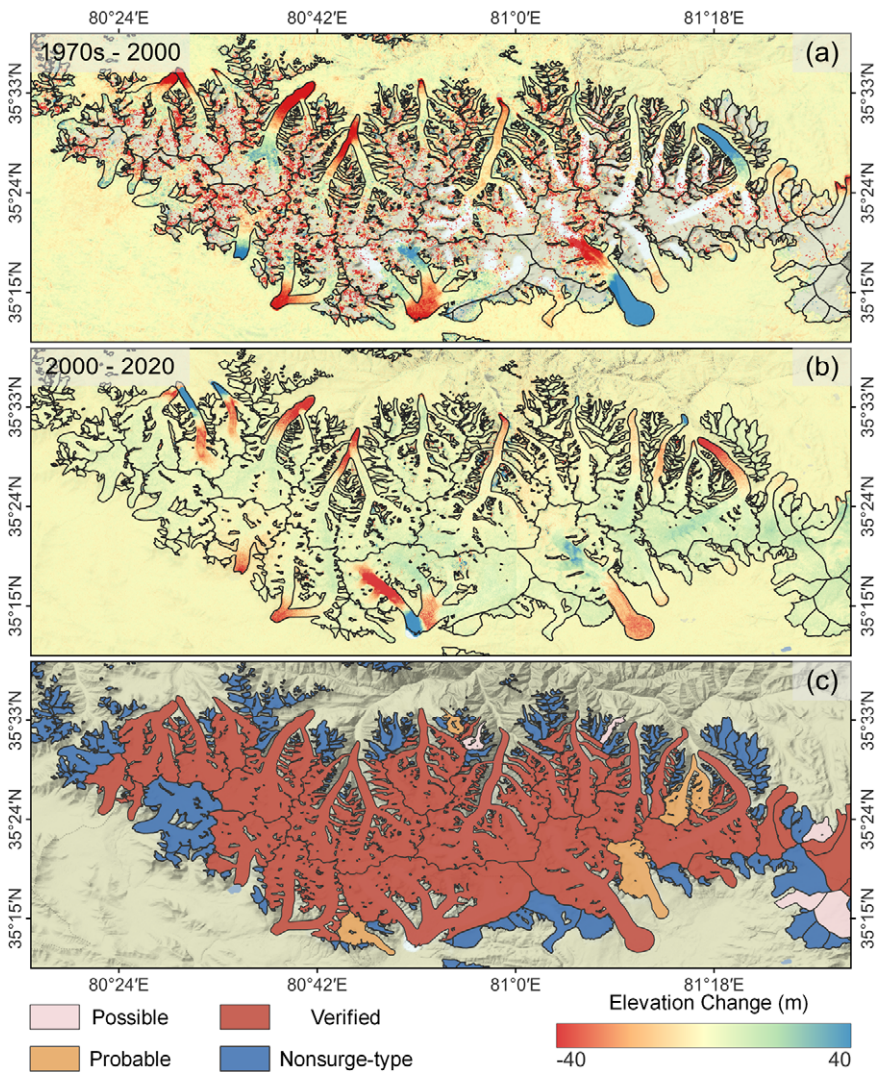
866

867

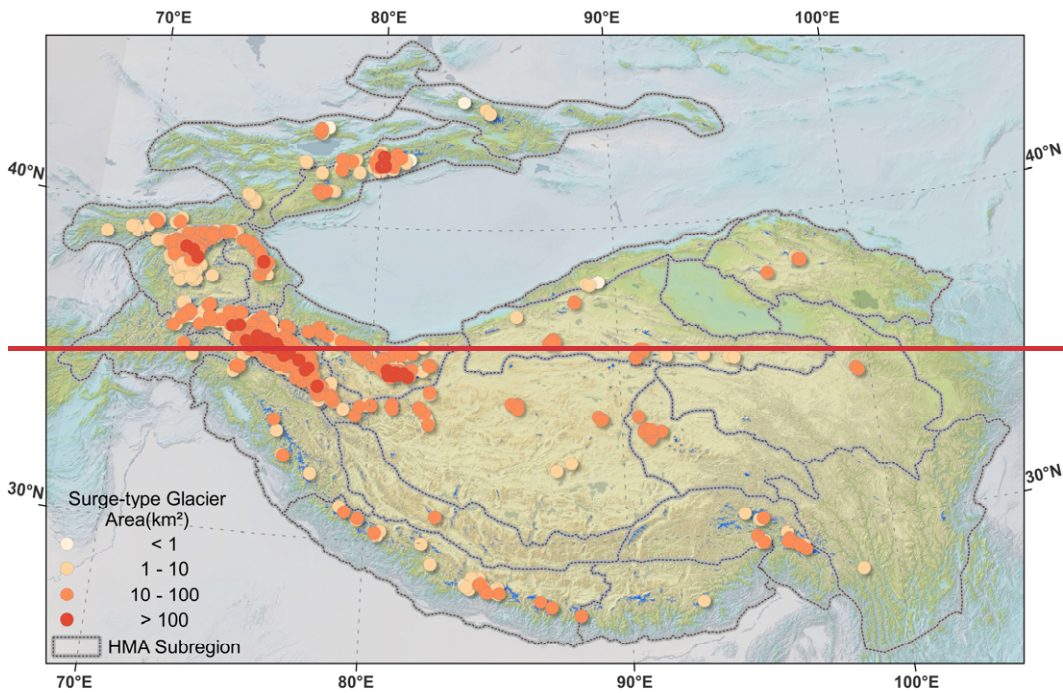
Figure 1: Footprints of (a) COP30/NASA DEMs, (b) HMA8m DEMs, and (c) KH-9 DEMs and (d) Landsat imageries that were utilized in this study. The background is rendered from the ESRI World Physical base map (Source: US National Park Service).

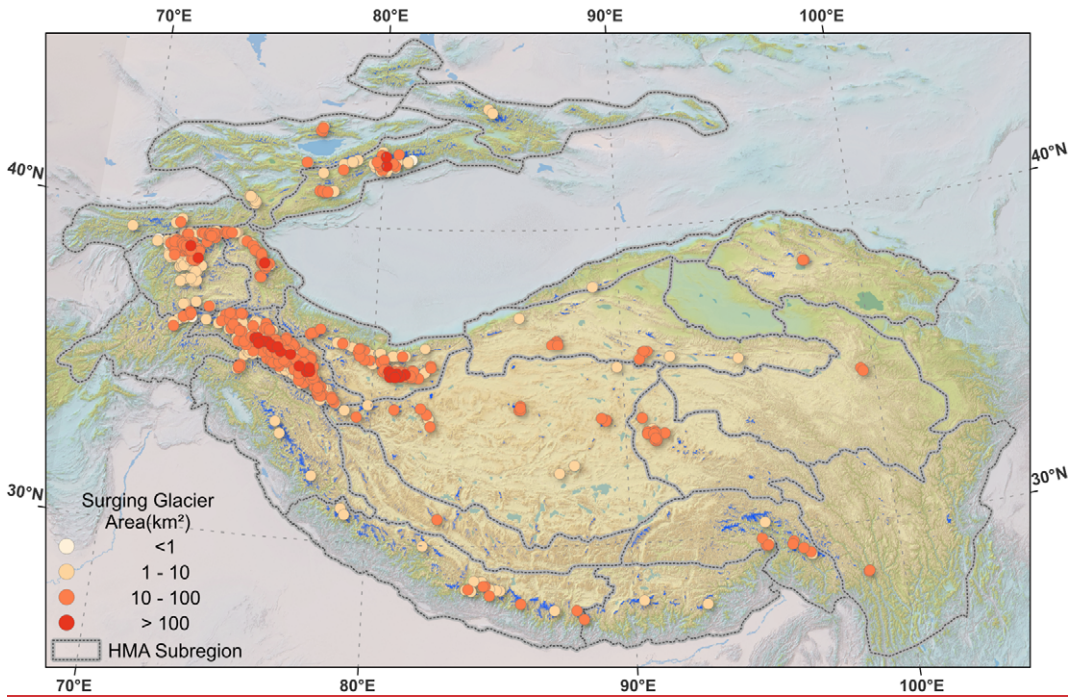


868



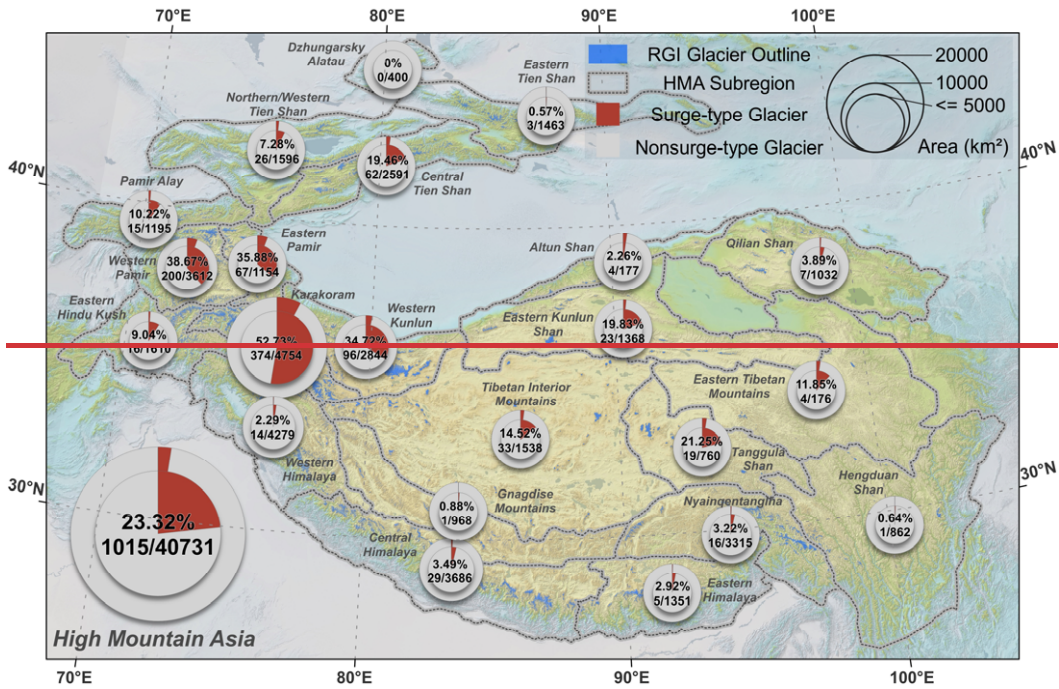
870 **Figure 2: An example of derived elevation change maps during 1970s-2000 (a) and 2000-2010s2020 (b), and the corresponding**
 871 **surge-typesurging** glacier identification result (c). Black curves are glacier outlines. The background is the shaded relief of COP30
 872 **DEM (Source: ESA). The area is located in the main massif of Western Kunlun Shan.**



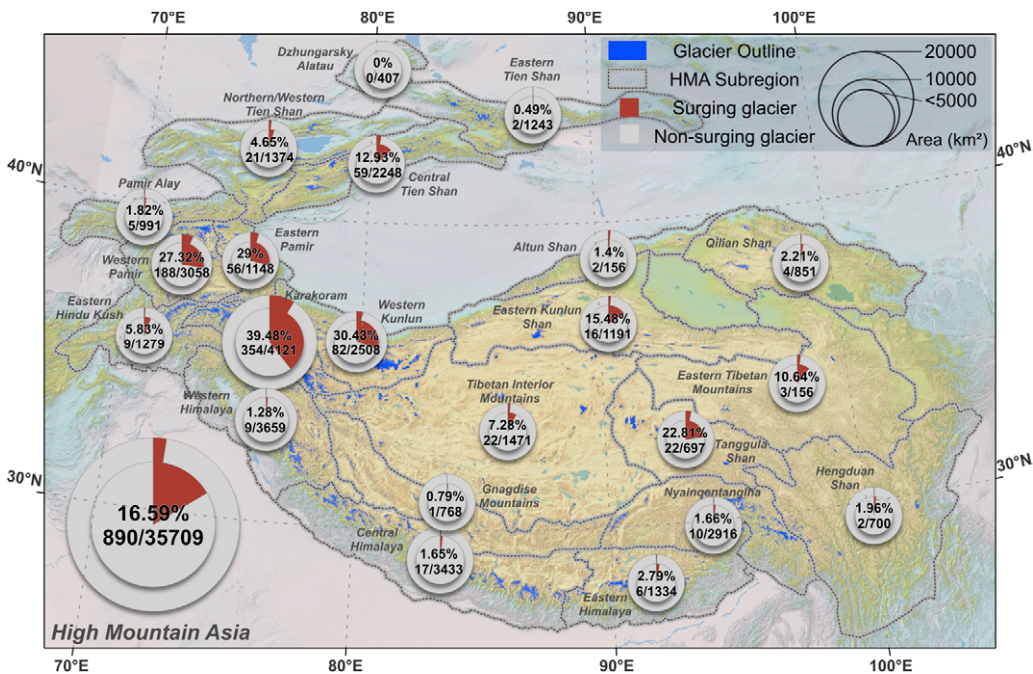


874

875 **Figure 3: Overview of the distribution of identified surge-type surge glaciers in 22 subregions of HMA. The background is the**
 876 **shaded relief of SRTM DEM (Source: USGS).**

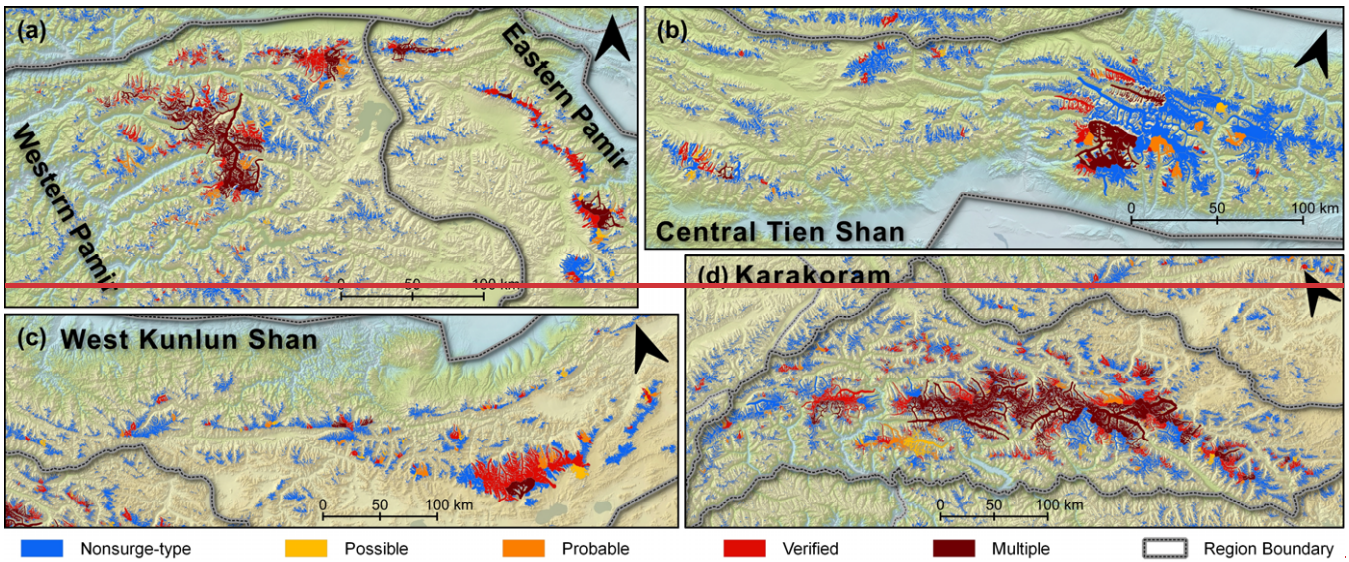


877

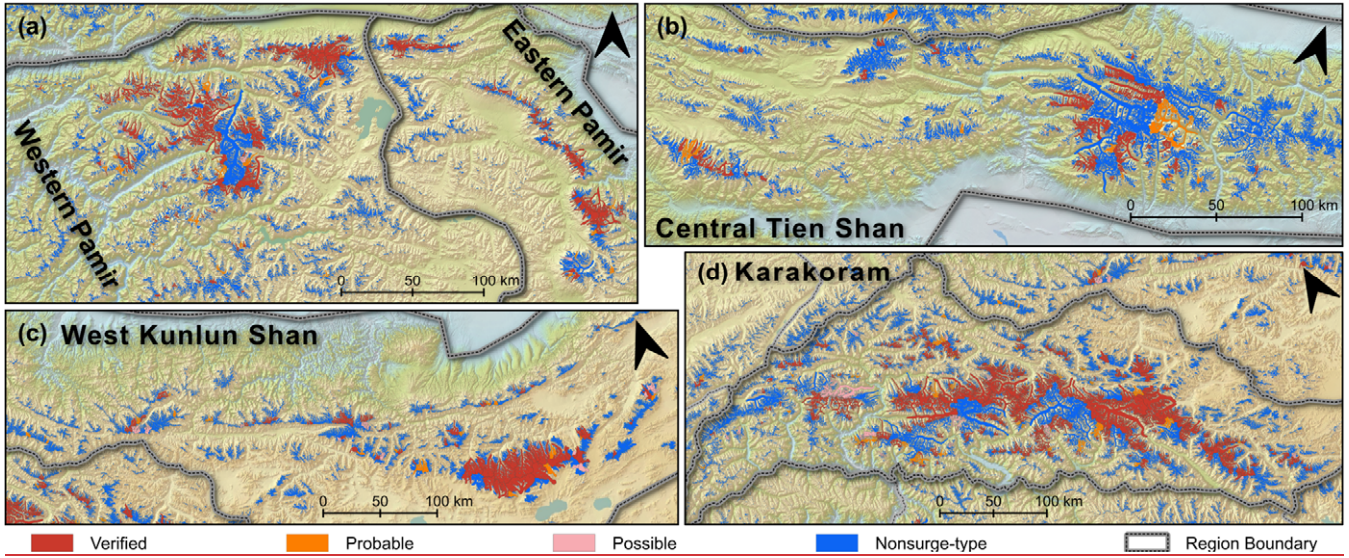


878

879 Figure 4: Distribution of **surge-type** glaciers in the 22 subregions of HMA. The double-level pie chart represents the ratios
 880 of **surge-type** glacier number and area in each subregion. The inner pie denotes the area ratio labelled by a percentage, and
 881 the outer pie denotes the number ratio labelled by a fraction (only considered glacier larger than 0.34 km^2). The background is the
 882 shaded relief of SRTM DEM (Source: USGS).

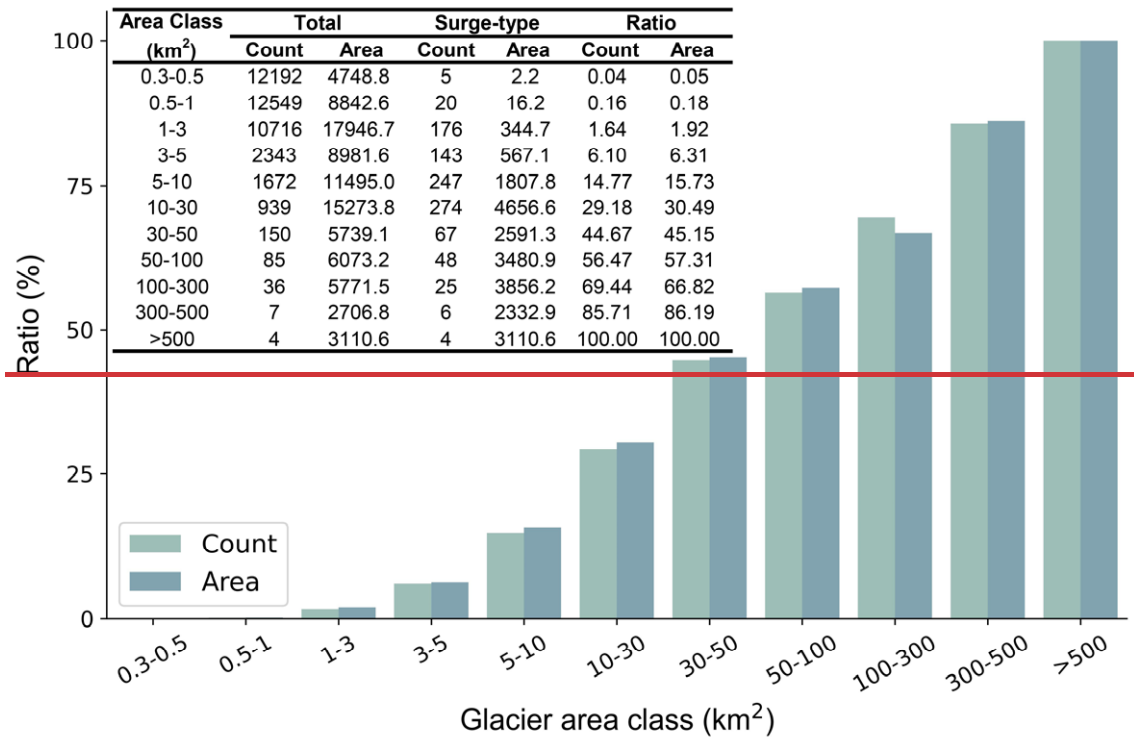


883



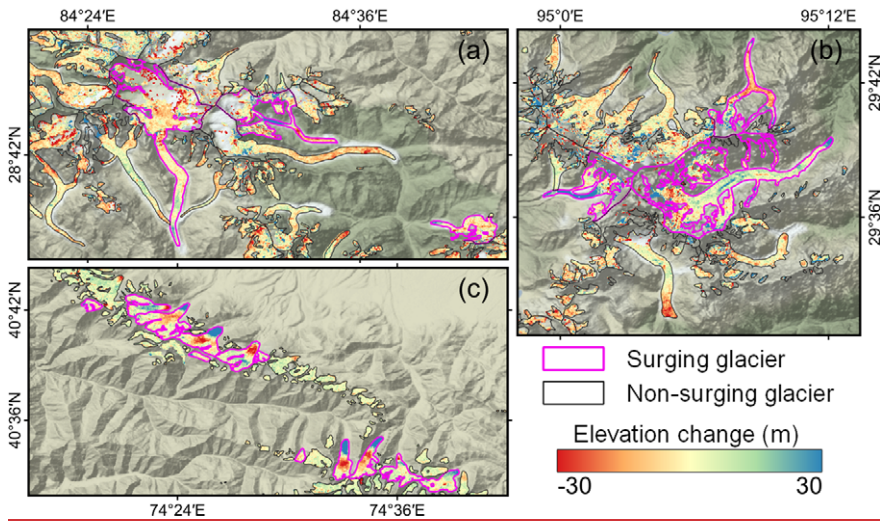
885

886 Figure 5: Results of surge-type glacier identification in the Pamirs (a), Central Tien Shan (b), West Kunlun Shan (c), and
 887 Karakoram (d). The background is the shaded relief of SRTM DEM (Source: USGS).



888

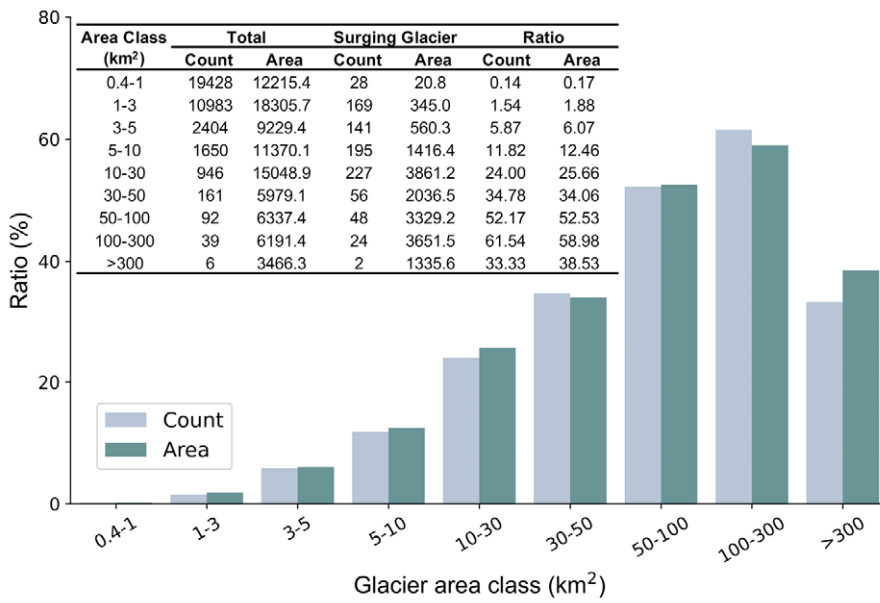
889



890

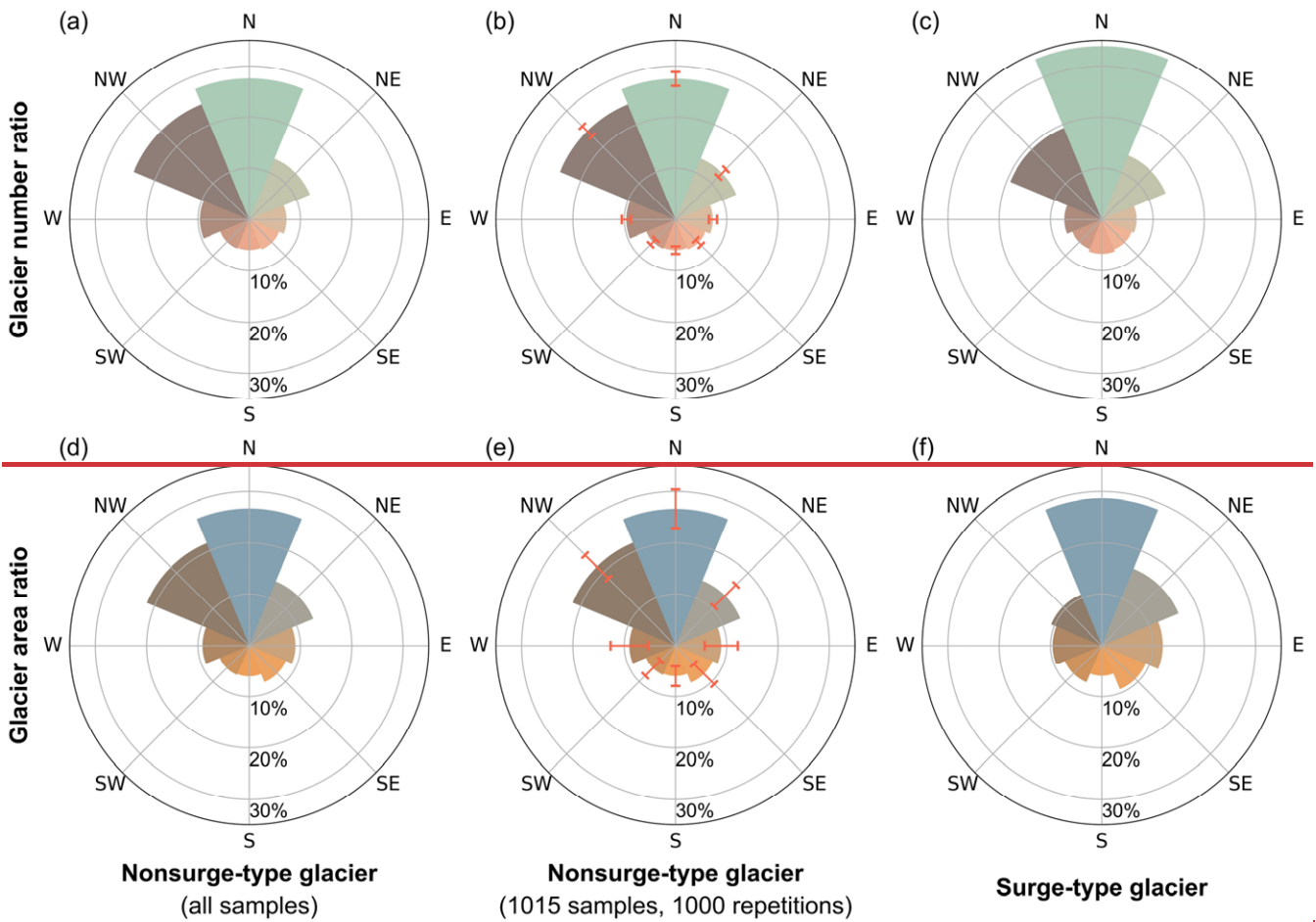
891 **Figure 6:** Elevation change map of identified surging glaciers samples in (a) Central Himalaya (1970s-2000) , (b) Nvainqentanglha
 892 (1970s-2000), and (c) Northern Western Tien Shan (2000-2020). Background is the shaded relief of SRTM DEM (Source: USGS).

893

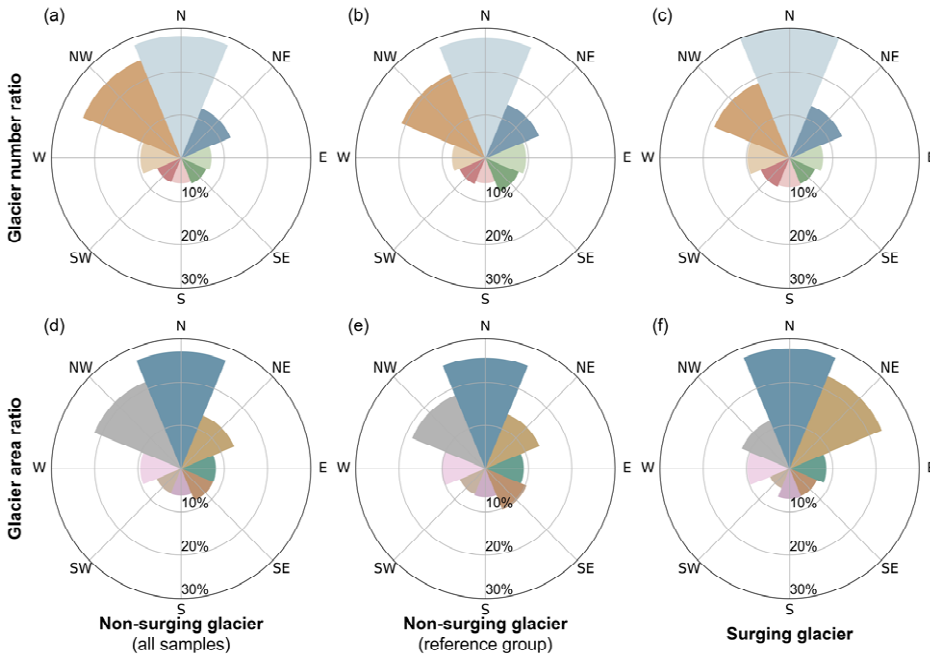


894

895 **Figure 7:** The ratios of surge-typesurging glacier number and area in different classes.



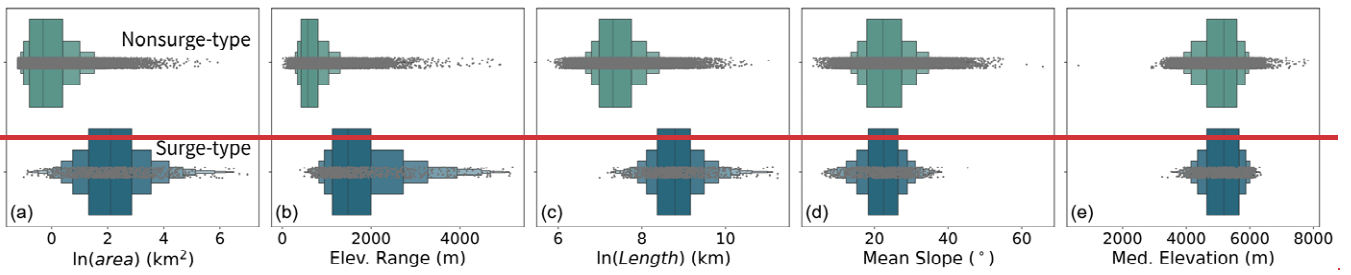
896



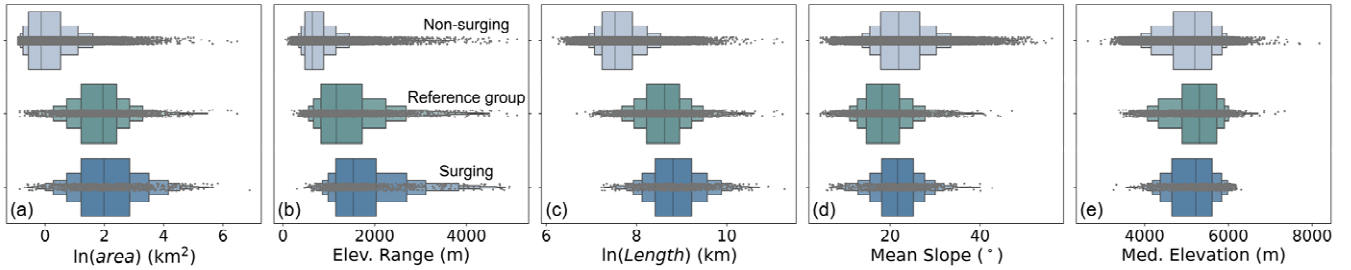
897

898 **Figure 78:** The distribution of glacier number and area in eight aspects. The upper row: glacier number ratio; lower row: glacier
 899 area ratio. Left column: distribution of all nonsurge-type glaciers; center column: averaged distribution of 1015 random
 900 nonsurge-type glacier samples with 1000 repetitions, the error bar denotes non-surging glaciers in the STD calculated from the 1000
 901 repetitions of nonsurge-type glacier samples reference group ; right column: distribution of surge-type glacier. Glaciers
 902 smaller than 0.34 km² were excluded in the nonsurge-type glaciers non-surging glacier class.

903



904



905

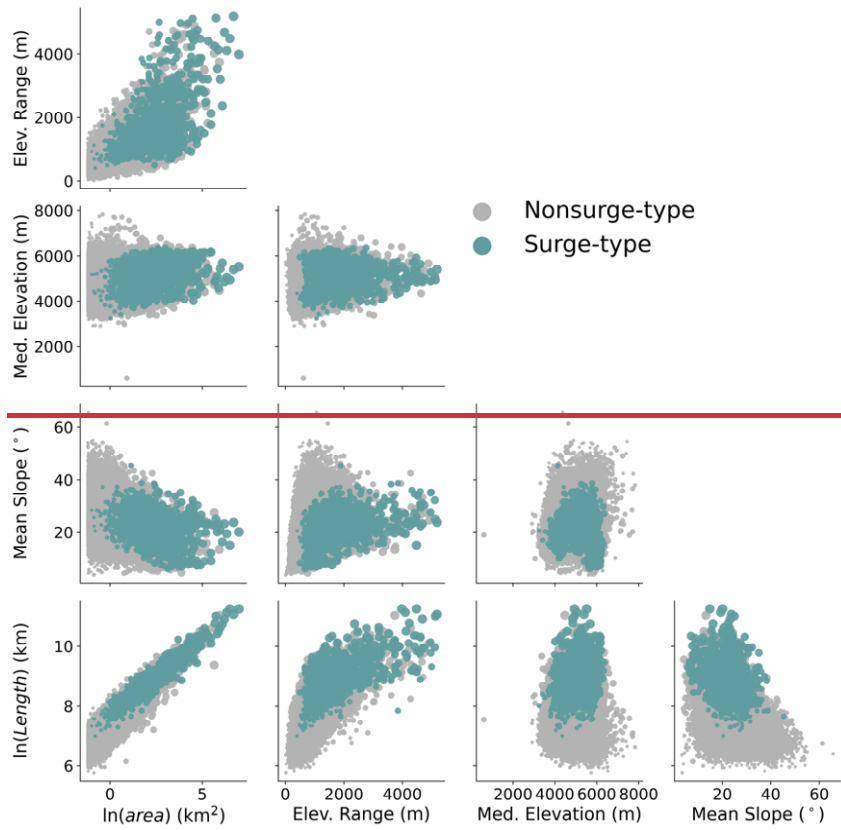
906

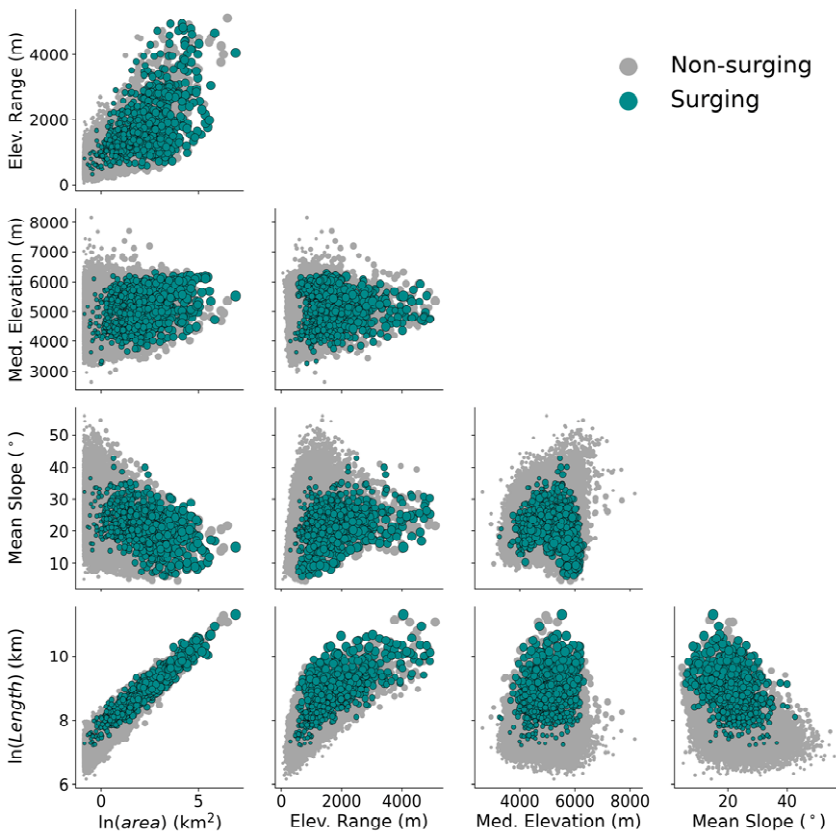
907

908

Figure 89: The comparison between the boxplots of geometric properties of **nonsurge-type and surge-type glaciers, non-surgings glaciers (top), non-surgings glaciers in reference group (center) and surging glaciers (bottom)**. (a) Natural logarithm of area. (b) elevation range. (c) Natural logarithm of length. (d) Mean surface slope. (e) Median elevation. Glaciers smaller than 0.34 km^2 were excluded in the **nonsurge-type glaciers** **non-surgings glacier** class.

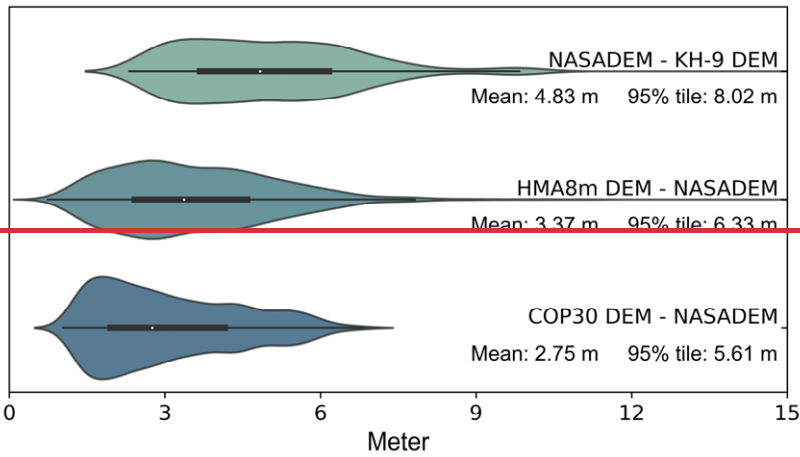
909





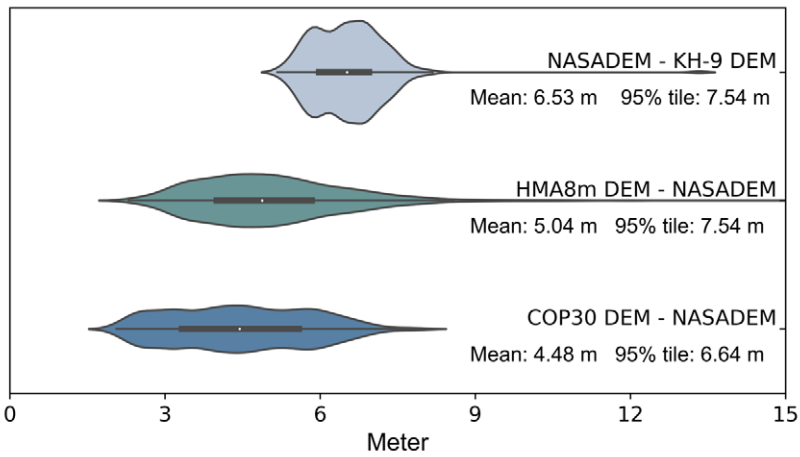
910

911 **Figure 910:** Bivariate scatterplots of geometric properties of ~~nonsurge-type~~non-surge and ~~surge-type~~surge glaciers. The larger
 912 dots represent larger glaciers. Glaciers smaller than 0.34 km² were excluded in the ~~nonsurge-type glaciers~~non-surge glacier class.



913

914



915

|916 **Figure 4011:** The distribution of NMAD of elevation change observations in stable areas of all DEM differencing tiles. In each
917 category, the shaded area denotes the density distribution of the NMAD of all DEM differencing tiles. The white dot denotes the
918 median in each group. The thick line represents the interquartile range (IQR, i.e., 75th percentile-25th percentile) in each group.
919 The thin line represents the range between the minimum value (25th percentile - 1.5IQR) and the maximum value (75th percentile
920 + 1.5IQR).